

Improved Polyakov-loop potential for effective models from functional calculations

Lisa M. Haas,^{1,2} Rainer Stiele,^{1,2} Jens Braun,^{3,2} Jan M. Pawłowski,^{1,2} and Jürgen Schaffner-Bielich^{1,2,4}

¹*Institut für Theoretische Physik, Universität Heidelberg,
Philosophenweg 16, D-69120 Heidelberg, Germany*

²*ExtreMe Matter Institute EMMI, GSI, Planckstraße 1, D-64291 Darmstadt, Germany*

³*Institut für Kernphysik (Theoriezentrum), Technische Universität Darmstadt,
Schloßgartenstraße 2, D-64289 Darmstadt, Germany*

⁴*Institut für Theoretische Physik, Goethe-Universität Frankfurt,
Max-von-Laue-Straße 1, D-60438 Frankfurt am Main, Germany*

(Dated: November 11, 2018)

We investigate the quark backreaction on the Polyakov loop and its impact on the thermodynamics of quantum chromodynamics. The dynamics of the gluons generating the Polyakov-loop potential is altered by the presence of dynamical quarks. However, this backreaction of the quarks has not yet been taken into account in Polyakov-loop extended model studies. In the present work, we show within a 2+1 flavour Polyakov-quark-meson model that a quark-improved Polyakov-loop potential leads to a smoother transition between the low-temperature hadronic phase and the high-temperature quark-gluon plasma phase. In particular, we discuss the dependence of our results on the remaining uncertainties that are the critical temperature and the parametrisation of the Polyakov-loop potential as well as the mass of the σ -meson.

PACS numbers: 25.75.Nq, 11.30.Rd, 12.38.Aw, 11.10.Wx, 11.15.Tk, 05.10.Cc

I. INTRODUCTION

Understanding the properties of the elementary particles in the phase diagram of strongly correlated matter is one of the major challenges of present research. Its general structure is dictated by the phase transition line separating the low-temperature hadronic phase associated with quark confinement and chiral symmetry breaking and the chirally symmetric high-temperature quark-gluon plasma phase. There are several possibilities to investigate this transition under different conditions. According to the standard model of particle physics and cosmology, this transition happened at least once and that is in the early Universe at high temperatures and small net quark densities (see e.g. Ref. [1]). Another natural environment where this transition might take place, now at high densities and low temperatures, could be supernovae and their remnants, compact stars (see e.g. Ref. [2]). More detailed information about the phase diagram can be obtained by large accelerator facilities with high performance detectors, as the Large Hadron Collider, the Relativistic Heavy Ion Collider, the Facility for Antiproton and Ion Research and the Nuclotron-based Ion Collider Facility (see e.g. Ref. [3]).

Functional continuum methods are well suited for a combined study of the chiral and confining dynamics of QCD at finite temperature and density. In recent years, much progress in this direction has been made within the functional renormalisation group (FRG) approach to QCD, see Refs. [4, 5], and to Polyakov-loop extended low-energy effective models, see Refs. [6–11]. In fact, the latter emerge dynamically from the first-principle QCD-flow at low energies: the parameters of these models defined below a hadronic mass scale ~ 1 GeV can be extracted from a QCD RG-flow starting with the classical QCD ac-

tion at a given high (perturbative) scale $\Lambda \gg \Lambda_{\text{QCD}}$. For the Polyakov-loop extended quark-meson model (PQM) this has been discussed in Refs. [5, 6, 8, 11].

Combining first-principle QCD flows with low-energy effective models can be very fruitful. For example, such an approach reveals the dynamical connection of confinement and chiral symmetry breaking from an analysis of the nonperturbative fixed-point structure of the theory, see Refs. [9, 10]. More generally, the first-principle determination of the input parameters of such models, as has been described above, can be used to systematically remove the ambiguities of low-energy effective models. This systematic procedure utilises the results of the first-principle flows for the chiral properties, see Refs. [4, 12–15], and confinement-deconfinement properties, see Refs. [4, 16–19], both in Yang-Mills (YM) theory and QCD at finite temperature and density. The technical details of this systematic embedding of low-energy effective models in first-principle QCD is discussed in Sec. II.

The embedding discussed above also entails that it is even more interesting to study low-energy effective models on their own in order to determine the relevant input parameters in these models, i.e., those the infrared behaviour of these models is sensitive to. Low-energy effective models capture the most important properties of strongly interacting matter and are well suited for basic investigations and applications, for a recent review see Ref. [20]. The most popular ones are the linear sigma model, also called quark-meson model in this context [21–32], the Nambu–Jona-Lasinio (NJL) model [33–37], and the Polyakov-loop extended versions thereof [6–8, 11, 38–50]. In these models the gauge part is adjusted to lattice calculations of Yang-Mills theory [40, 44, 46]. A first step towards the full inclusion of the backreactions of quarks

on the gauge sector is to estimate the change of the transition temperature of the Polyakov-loop potential when going from Yang-Mills theory to QCD [6]. This can safely be done on the basis of a perturbative estimate of the change of Λ_{QCD} when going from Yang-Mills theory to QCD [6] which also has been used for the chiral dynamics [13, 14]. However, on the mean field level such an analysis lacks the full inclusion of glue-matter dynamics to both the chiral as well as the confinement-deconfinement physics. The related quantum and thermal fluctuations typically smoothen the respective phase transitions. Indeed, the mean field models show sharper transitions in comparison to the full theory, see Ref. [4]. In the present work, we will show that the functional renormalisation group allows for a comparison of the Yang-Mills potential with the glue part of the full effective potential in QCD. We extract the relation of both and apply it then to improve the Polyakov-loop potential entering effective models, such as Polyakov-loop extended Nambu–Jona-Lasinio/quark-meson (PNJL/PQM) models. With this improved Polyakov-loop potential we shall see that the phase transition becomes smoother and is in better agreement with most recent results from functional QCD studies and lattice QCD simulations.

The paper is organised as follows: in the following section II we summarise our results from a functional renormalisation group approach which we have already used in earlier studies to compute the Polyakov-loop potential. In particular, we compare in Sec. IIB the pure Yang-Mills potential with the glue part of the full effective potential in QCD. From this comparison, we extract a description of how the pure Yang-Mills Polyakov-loop potential entering PNJL/PQM models has to be modified such that the quark backreaction on the gluodynamics generating this potential is effectively taken into account. After we have given a brief summary of the PQM model in Sec. III, we employ our results from Sec. IIB to amend the Polyakov-loop potential entering PNJL/PQM model studies. In Sec. IV, we then show how this improvement affects the temperature dependence of the order parameters and thermodynamic observables, in particular close to the phase transition. To complete our studies we discuss the dependence of our results on the remaining free parameters. Finally, in Sec. V, we give our conclusions and outline possible continuations.



FIG. 1. Partially hadronised version of the FRG flow for QCD. The loops denote the gluon, ghost, quark and hadronic contributions, respectively. The crosses mark the RG regulator term.

II. FUNCTIONAL FLOWS IN QCD & LOW ENERGY EFFECTIVE MODELS

It has been known since long, see e.g. Refs. [4–6, 8, 15, 27, 51–54], that low-energy effective models can be systematically related to full QCD within the FRG-approach. For Polyakov-loop extended models this follows from the Landau gauge approach in Refs. [4, 5, 55], for the Polyakov gauge see Refs. [17, 56]. This setting has been discussed in details for the PQM model in Refs. [5, 8, 11, 57]. While chiral symmetry and its dynamical breaking are well described within these models, confinement is only included in a statistical manner via a phenomenological Polyakov-loop potential \mathcal{U} . This potential is fixed to lattice data of the pure Yang-Mills system at vanishing chemical potential, hence it is approximately the Polyakov loop potential in Yang-Mills theory, V_{YM} . More specifically, a Polyakov-loop potential is embedded in these models which reproduces the temperature dependence of the Polyakov loop and the thermodynamics of pure Yang-Mills theory as obtained in lattice simulations. As this only fits two observables which basically do not change below the phase transition, this leaves us with a big parameter space. Results for the different potentials have e.g. been discussed in Refs. [48, 50]. Also, the coupling of the matter sector to the gauge sector is lost in such an approach, see also the discussion in Refs. [5, 6, 8, 11, 57].

In summary this entails that the glue potential of full QCD, V_{glue} , encoding the gauge dynamics in the presence of matter fields, is replaced by a phenomenological Polyakov-loop potential \mathcal{U} . The present work is based on a qualitative improvement of this approximation towards full QCD by embedding Polyakov loop extended models within QCD flows.

A. QCD with functional methods

In this section we summarise results obtained with functional methods for QCD. The present work mostly relies on the results obtained in Refs. [4, 5] for the QCD phase diagram. In Ref. [4] the FRG approach to the phase diagram was put forward on the basis of the QCD flow equation in the background Landau gauge (Landau-DeWitt). It is governed by the flow for the QCD effective action $\Gamma_k[\bar{A}; \phi]$,

$$\begin{aligned} \partial_t \Gamma_k[\bar{A}; \phi] = & \frac{1}{2} \text{Tr} G_a[\bar{A}; \phi] \partial_t R_A - \text{Tr} G_c[\bar{A}; \phi] \partial_t R_c \\ & - \text{Tr} G_q[\bar{A}; \phi] \partial_t R_q + \frac{1}{2} \text{Tr} G_H[\bar{A}; \phi] \partial_t R_H, \quad (1) \end{aligned}$$

depicted in Fig. 1. Here, \bar{A} is the gluonic background and $\phi = (a, c, \bar{c}, q, \bar{q}, \text{hadrons})$ are the dynamical fluctuations with $A = \bar{A} + a$. The flow (1) of the effective action or free energy only depends on the full field-dependent fluctuation propagators $G_\phi[\bar{A}; \phi]$,

$$G_\phi[\bar{A}; \phi](p, q) = \left(\frac{1}{\Gamma_k^{(2)}[\phi] + R_k} \right)_{\phi\phi}(p, q), \quad (2)$$

and the regulator functions R_ϕ . The regulators R_ϕ depend on background covariant momenta $\bar{D} = \partial - i g \bar{A}$ such that for small momenta it acts as a mass and for large momenta it vanishes sufficiently fast; i.e., R_k acts as a momentum-dependent additional mass term. The present approach has the advantage that hadronic states can be included successively within dynamical hadronisation, see Refs. [51, 52, 58, 59]. This simply entails that part of the quark and gluonic fluctuations are treated separately as they carry hadronic resonances. It is worth emphasising that this is done dynamically within the QCD-setting so there is no danger of overcounting terms present within an effective model setup. The QCD results obtained in the present work are computed within the approximation to two-flavour QCD detailed in Refs. [4, 5] which explicitly takes into account the lowest mesonic multiplet, the σ -meson and the pions, $\sigma, \vec{\pi}$.

The FRG-approach to QCD outlined above as well as other functional approaches allow us to access the physics of the confinement-deconfinement phase transition in a simple way, see Refs. [4, 5, 16, 18, 19]. The symmetry behind this transition, the center symmetry, is only an unbroken symmetry for infinitely heavy quarks. Then, QCD reduces to a pure $SU(N_c)$ gauge theory. The commonly used order parameter is the expectation value of the Polyakov-loop operator,

$$\begin{aligned} \Phi(\vec{x}) &\equiv \Phi[A(\vec{x})] \\ &= \frac{1}{N_c} \text{tr}_c \left[\mathcal{P} \exp \left(i \bar{g} \int_0^\beta dx_0 A_0(x_0, \vec{x}) \right) \right], \quad (3) \end{aligned}$$

where $\beta = 1/T$ is the inverse temperature, \bar{g} denotes the bare gauge coupling and \mathcal{P} stands for path ordering. The Polyakov loop is then given by $\langle \Phi(\vec{x}) \rangle$.

Strictly speaking, the Polyakov loop $\langle \Phi(\vec{x}) \rangle$ is an order parameter for center symmetry breaking, see e.g. Ref. [60]. However, its logarithm can be associated to half of the free energy $F_{q\bar{q}}$ of a quark-antiquark pair at infinite distance. A center-symmetric confining phase is indicated by a vanishing Polyakov loop and implies that the free energy of a static quark is infinite. On the other hand, the deconfined phase is associated with a finite free energy of a static quark and, in turn, a finite Polyakov loop. The latter implies that center symmetry is broken spontaneously at high temperatures in Yang-Mills theories. In the presence of (light) dynamical quarks, the Polyakov loop is then finite for all temperatures but still becomes small in the ‘‘confined’’ low-temperature phase. This can be eventually traced back to the fact that quarks explicitly break the (global) center symmetry of the theory.

In addition to the standard Polyakov loop, other order parameters for quark confinement have been introduced. In this work we shall consider an order parameter which is closely related to the Polyakov loop, namely $\Phi[\langle A_0 \rangle]$. In

Polyakov-Landau-DeWitt gauge, it can be indeed shown that $\Phi[\langle A_0 \rangle]$ also is an order parameter, see Refs. [16, 17]. Here, $\langle A_0 \rangle$ is a constant element of the Cartan subalgebra of the gauge group and denotes the ground state of the order-parameter potential which is the Polyakov-loop potential. Perturbatively, the related effective potential $V[\langle A_0 \rangle]$ has first been computed in Refs. [61, 62].

Based on a functional RG approach, first nonperturbative QCD studies of this potential, including a computation of the phase transition temperatures for $SU(N_c)$ Yang-Mills theories, have been presented in Refs. [16–18]. In Ref. [19] the computation has been extended to general functional methods, i.e., Dyson-Schwinger equations and the 2PI-approach using the thermal propagators obtained in Refs. [63, 64]. In Refs. [4, 5] the approach has been applied to $N_f = 2$ QCD in the chiral limit. This computation within two-flavour QCD includes the full backcoupling of the matter sector on the propagators of the gauge degrees of freedom via dynamical quark-gluon interactions [14, 15, 51]. In particular, this includes the resolution of the full momentum dependence of the ghost and gluon propagators [63–69]. Recently, the nonperturbative Polyakov-loop potential has also been studied using various other approaches [70–76].

In the present work, we refrain from repeating the details of the above works but only refer to it whenever it is required. For general QCD-related introductions and reviews to our functional RG approach, we refer the reader to Refs. [5, 27, 52–54, 77, 78].

B. From QCD to Polyakov-loop extended chiral models

For temperatures below the chiral and confinement-deconfinement phase transitions the glue dynamics decouples from the matter dynamics. In the Landau gauge this physical decoupling is realised simply by a mass gap in the gluon propagator, that is $p^2 G_a(p^2) \rightarrow 0$ for small momenta, see e.g. Ref. [69] and references therein. As the ghost-matter coupling is mediated by the gluon this decoupling extends to the full ghost-gluon dynamics. Hence the pure glue sector of the theory decouples as expected, and the QCD flow equation reduces to

$$\partial_t \Gamma_k[\bar{A}; \phi] = -\text{Tr} G_q[\bar{A}; \phi] \partial_t R_q + \frac{1}{2} \text{Tr} G_H[\bar{A}; \phi] \partial_t R_H, \quad (4)$$

which is depicted in Fig. 2. The background gluon field as well as the ghost and gluon fluctuation fields A and c, \bar{c} are simply spectators in Eq. (4). If setting the spectator fields to zero the flow equation (4) reduces to that of generic low-energy models of QCD. The respective models are then singled out by specifying the hadronic content of the flow. In Eq. (4), the presence of a quark loop should not be confused with the presence of quarks as observable (asymptotic) states. The presence of this loop only states that quark loops are still present ‘‘internally’’ and required to give a microscopic description of the in-

FIG. 2. FRG flow for the matter sector of QCD. The loops denote the quark and hadronic contributions, respectively. The crosses mark the RG regulator term.

teraction of the hadronic degrees of freedom. In the same spirit, gluon loops also play a role in the low-energy sector even though they do not represent observable (asymptotic) states in this regime as well. However, gluon loops govern the dynamics of the confinement order-parameter potential which in turn determines the background gluon field entering Eq. (4), see also our discussion below.

The most prominent example are NJL-type models. In these models the hadronic loops are missing completely and the full matter dynamics is described by the quark loop. This is in correspondence to a description of the low-energy matter dynamics of QCD purely in terms of quark correlation functions. This only captures the correct QCD-dynamics if the hadronic spectrum is taken into account via resonances in the scattering amplitudes of quarks, e.g. in the quark-quark scattering kernel. The latter is directly related to the four point function $\Gamma^{(4)}$ of two quark-antiquark pairs. It is worth noting in this context that the flow equation (4) includes vertex and propagator corrections to the theory and hence naturally incorporates the so-called nonlocal NJL models [56, 79, 80]. For a detailed discussion of the presence and emergence of nonlocal fermionic vertices in RG flows, we refer the reader to Ref. [54].

Even though this incorporates in principle the full dynamics, hadronic contributions are more easily taken into account via (dynamical) hadronisation, see Refs. [15, 51, 52, 58, 59]. This technique describes the following physical mechanism: when lowering the RG-scale in the QCD flow equation (1), Fig. 1, strongly-bound quark correlations e.g. quark-antiquark (mesons), diquark, and three-quark (baryons) correlations, will be dynamically created by the flow. These correlations can be parameterised in terms of mesonic, diquark and hadronic operators respectively. Note that the diquark operators do not describe asymptotic states but intermediate correlations. The respective coupling of the hadronic operators is dynamically enhanced by the quark-gluon fluctuations at higher scales, while it takes over the dynamics from the quark-gluon sector at lower scales, hence the name dynamical hadronisation. This fluctuation-triggered hadronisation within the QCD-flow clearly avoids any double-counting problem: the hadrons are created dynamically, the respective couplings are created from the QCD input which only depends on a single input parameter, the strong coupling α_s .

Quantum and thermal fluctuations are self-consistently taken into account. Still, at low scales, say for $k \lesssim 1$ GeV, the pure glue sector decouples and we are left with Eq. (4). Note that within such a procedure the initial effective action Γ_Λ at $\Lambda \approx 1$ GeV serves as the classical action of the quark-hadronic low-energy model and its coupling constants are directly derived from QCD.

In the present work we consider such a quark-hadronic model at finite temperature and vanishing density: close to the phase boundary between the quark-gluon plasma phase and the hadronic phase and at not too large chemical potential mesonic degrees of freedom, in particular the pion and σ -fluctuations, become important. Here, we assume that the associated bosonic fields can be described as composites of fermions and do not carry an internal charge, such as colour or flavour: $\sigma \sim \bar{q}q$ and $\vec{\pi} \sim \bar{q}\gamma_5\tau q$. A priori, these fields are just auxiliary fields introduced by means of a Hubbard-Stratonovich transformation of a purely fermionic theory. Since these composite objects have considerable overlap with the full meson operators, they are well suited to describe the meson dynamics in a first approximation. Keeping this in mind, the (effective) action of QCD can be expanded in powers of these mesonic operators, at least for small momentum scales. Momentum dependencies and corrections of higher order can conveniently and systematically be taken into account, e.g., by means of a derivative expansion of the effective action, see Ref. [54] for a review. In the fully coupled QCD RG-flow, the strength and the momentum dependence of the various couplings can then be derived from the microscopic QCD action. In fact, the loops depicted in Fig. 1 are intrinsically coupled to each other. In particular, there are contributions from the matter sector to the diagrams for the gluon propagator, i.e., the quark part of the gluonic vacuum polarisation, see Fig. 4.

Hence we only take into account mesonic correlations in terms of effective operators. Baryonic fluctuations are considered as subleading at vanishing density and are partially taken into account in the quark correlations. Moreover, the gluonic background is determined by the constant solution of the QCD equations of motion. Such a solution can always be rotated in the Cartan,

$$\langle A_\mu \rangle = \delta_{\mu 0} \langle A_0^3 \rangle \tau^3 + \langle A_0^8 \rangle \tau^8, \quad (5)$$

with constant $\langle A_0^{3,8} \rangle$. The minima and maxima of the potential are accessed for $\langle A_0^8 \rangle = 0$, see Refs. [4, 16–19]. Then the Polyakov loop reads

$$\Phi[A_0] = \frac{1}{3} \left[1 + 2 \cos \left(\frac{1}{2} \beta g A_0 \right) \right], \quad \text{with } A_0 = \langle A_0^3 \rangle \quad (6)$$

In summary this leads to quark-meson flows (4) in constant temporal gauge field backgrounds which define the PQM model [6], including its matter quantum and thermal fluctuations. We note that for the NJL-type model this defines the PNJL model including its quantum and thermal fluctuations. The generalised version is the Polyakov-loop extended quark-hadron (PQH) model.

$$\partial_t \Gamma_k[\bar{A}; \phi] = \frac{1}{2} \left(\text{diagram with two loops and a regulator insertion} \right) - \text{diagram with one loop and a regulator insertion}$$

FIG. 3. Functional flow for the effective action. Lines with filled circles denote fully dressed field-dependent propagators (2). Crossed circles denote the regulator insertion $\partial_t R_k$.

Even though the glue-dynamics decouples for low temperatures, the gluonic background $\bar{A} = \langle A \rangle$ does play an important rôle. In the confining phase it screens the propagation of the quarks which confines them even statistically, leave aside the confining potential. The expectation value $\langle A \rangle$ is given by the solution of the QCD equations of motion which also requires the first part of the QCD flow, that is

$$\partial_t \Gamma_k[\bar{A}; \phi] = \frac{1}{2} \text{Tr} G_a[\bar{A}; \phi] \partial_t R_A - \text{Tr} G_c[\bar{A}; \phi] \partial_t R_c. \quad (7)$$

depicted in Fig. 3. The fluctuation ϕ is evaluated at the equation of motion (EoM), $\phi = \bar{\phi}$: the gluonic fluctuation background is vanishing, $\bar{a} = 0$, whereas the mesonic background is given by $\sigma = \bar{\sigma}$ and $\vec{\pi} = 0$ leading to the running quark masses in the quark vacuum polarisation depicted in Fig. 4. This leads us finally to

$$\partial_t V_{\text{glue}}[A_0] = \frac{1}{\beta \mathcal{V}} \partial_t \Gamma_k[A_0; \bar{\phi}], \quad (8)$$

for constant backgrounds A_0 and spatial volume \mathcal{V} . Structurally, Eq. (7) resembles the pure Yang-Mills flow equation,

$$\partial_t V_{\text{YM}}[A_0] = \frac{1}{\beta \mathcal{V}} \partial_t \Gamma_{\text{YM},k}[A_0; a = 0, C = 0, \bar{C} = 0], \quad (9)$$

which also has the pictorial form of Fig. 3. The ghost and gluon propagators in Eq. (8), however, are those of QCD. In particular, the flow of the gluon propagator receives contributions from matter loops, e.g. the quark contribution to the vacuum polarisation, see Fig. 4.

It has been already mentioned at the beginning of this section that in the standard approach to Polyakov-loop extended models the glue potential V_{glue} in Eq. (8) is approximated by an approximation to its Yang-Mills analogue, V_{YM} in Eq. (9). To bring these studies closer to (full) QCD, however, this Polyakov-loop potential effectively generated by pure gluodynamics has to be replaced by the QCD glue potential, i.e., by the contribution stemming from the gauge degrees of freedom in the presence

$$\partial_t \Pi_{A,k}^{\text{ferm}} \simeq \text{diagram showing a quark loop with a regulator insertion}$$

FIG. 4. Quark polarisation contribution to the gluon propagator representing a contribution to the matter backcoupling.

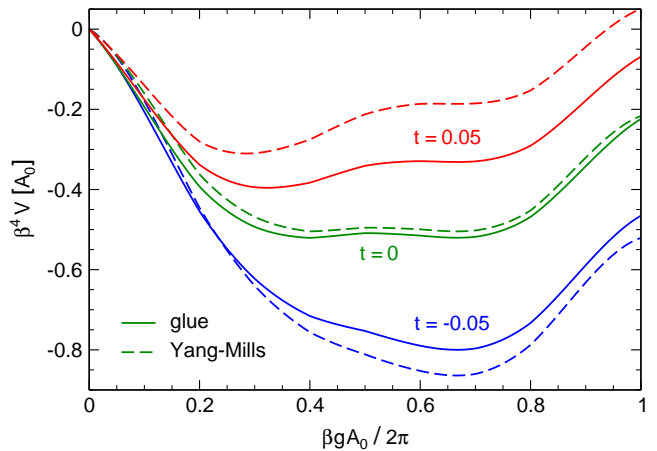


FIG. 5. Comparison of the SU(3) Yang-Mills and glue effective potentials as functions of the background gauge field $A_0 = \langle A_0^3 \rangle$ for various reduced temperatures, see the text for the definition of the reduced temperatures. The form of the potentials is very similar, however, the temperature scale changes. Only the glue part of the full effective potential is shown here and compared to the Yang-Mills potential.

of dynamical quarks. It is therefore beneficial to amend these model calculations by utilising the available information on this glue part of the potential.

In the present work, we only consider Polyakov-loop potentials which have been computed by considering two quark flavours with vanishing current masses. The strange quark has been ignored. We expect that the corrections resulting from the inclusion of a strange quark are subleading in our present studies. Following Refs. [4, 16–19], we have computed the nonperturbative Polyakov-loop potential using the above mentioned functional RG approach taking into account the back-reaction of the quark degrees of freedom on the gluon propagators[4].

In Fig. 5, we compare the effective potential of SU(3) Yang-Mills theory as obtained in Refs. [16, 18, 19] with the Polyakov-loop potential of the glue sector of our present study. The latter includes also the quark part of the gluonic vacuum polarisation but does not include the fermionic part of the full potential. The related order-parameters $\Phi[\langle A_0 \rangle]$ derive by inserting the temperature-dependent gauge field value at the minimum into Eq. (6). The order parameter shows a first-order phase transition for both, the glue potential and the Yang-Mills potential. It is displayed for Yang-Mills theory in Fig. 6. We observe immediately in Fig. 5 that the temperature scale of the various Yang-Mills potentials and the glue potentials differ. The differences are induced by the matter fluctuations altering the propagators of the gauge fields. This has already been anticipated in Ref. [6], where a phenomenological hard-thermal-loop (HTL) estimate led to $T_{\text{cr}}^{\text{HTL}} = 208$ MeV for two quark flavours.

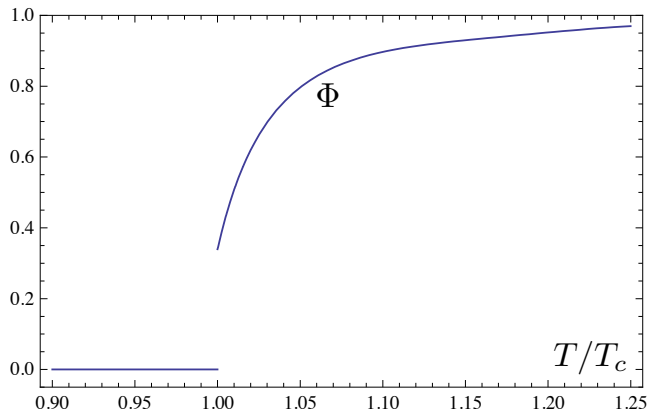


FIG. 6. Yang-Mills order-parameter $\Phi[\langle A_0 \rangle]$ as a function of the normalised temperature T/T_c with $T_c = 276 \text{ MeV}$.

Although the temperature scales are different, the shape of the order-parameter potential V is not, see Fig. 5. We can exploit this observation to estimate how the temperature of a given pure Yang-Mills Polyakov-loop potential has to be modified to be closer to the QCD potential. To this end, we need to define a measure for the comparison of the potentials. We use

$$\int_0^{\frac{2\pi T}{g}} dA_0 |V_{\text{YM}}(A_0) - V_{\text{glue}}(A_0)|^2. \quad (10)$$

Moreover, we introduce the reduced temperatures

$$t_{\text{glue}} = \frac{T - T_{\text{cr}}^{\text{glue}}}{T_{\text{cr}}^{\text{glue}}}, \quad t_{\text{YM}} = \frac{T - T_{\text{cr}}^{\text{YM}}}{T_{\text{cr}}^{\text{YM}}}, \quad (11)$$

where $T_{\text{cr}}^{\text{glue}} = 203 \text{ MeV}$. Note that this is not the critical temperature obtained from the full effective potential including pure quark loops but only from the contribution stemming from the glue part of the potential for two massless quark flavours [4]. We add that the absolute scale in Ref. [4] was not computed in a chiral extrapolation of the theory with physical quark masses. Hence, in the applications to the PQM model we will leave the glue critical temperature as a free parameter, maximally ranging from

$$180 \text{ MeV} \lesssim T_{\text{cr}}^{\text{glue}} \lesssim 270 \text{ MeV}. \quad (12)$$

The upper limit in Eq. (12) is the critical temperature of Yang-Mills theory, the lower limit is the estimate in Ref. [6], see also Table I. For $T_{\text{cr}}^{\text{YM}}$, on the other hand,

TABLE I. Critical temperature of the glue effective potential $T_{\text{cr}}^{\text{glue}}$ for N_f massless flavours and in case of an additional massive quark flavour with the current strange quark mass of 95 MeV [81], according to Ref. [6].

N_f	0	1	2	3	2 + 1
$T_{\text{cr}}^{\text{glue}}$ [MeV]	270	239	208	178	182

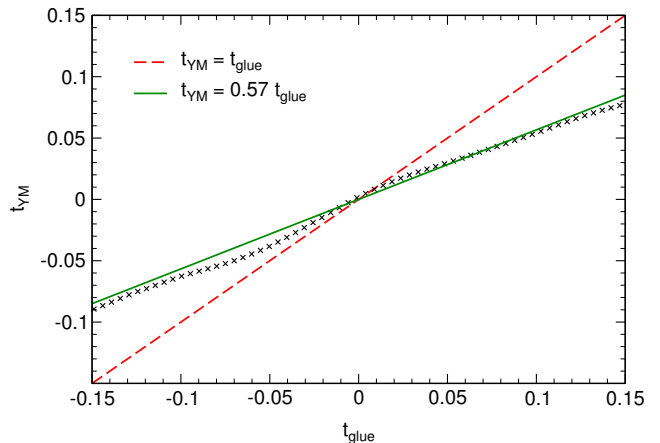


FIG. 7. Relation between the two temperature scales of pure Yang-Mills theory and the glue part of our present study including the backreaction of the quarks on the gauge fields. The solid (green) line is our fit to the numerical data (black crosses) in the range around the transition temperatures. A clear deviation from linear behaviour with slope one (dashed red line), i.e., data from pure Yang-Mills theory, can be recognised.

we find $T_{\text{cr}}^{\text{YM}} = 276 \text{ MeV}$ [16, 18, 19] which is in quantitative agreement with the results from lattice studies. The comparison of the potentials then yields the translation of the two temperature scales: given a reduced QCD-temperature t_{glue} , the related Yang-Mills temperature t_{YM} is that which minimises Eq. (10). This leads to

$$t_{\text{YM}}(t_{\text{glue}}) \approx 0.57 t_{\text{glue}}, \quad (13)$$

which, together with the absolute temperature scale in Eq. (12) serves as an important input for model studies. This relation is displayed in Fig. 7. Equation (13) also provides the map from the temperature-dependence of the Yang-Mills order-parameter to that derived from the glue potential by using $t_{\text{YM}}(t_{\text{glue}})$ in Fig. 6. The respective order-parameter flattens, but still shows a first-order transition. This procedure also extends to finite chemical potential e.g. with the chemical potential dependence in Ref. [6]. A refinement of this estimate based on full QCD flows, which obeys the Silver-Blaze property for vanishing temperature, is derived in Ref. [11]. Note also that the approximation (13) holds only for small and moderate temperatures, as at high scales the slope of Eq. (13) saturates, where one reaches the perturbative limit and the potentials reach their asymptotic form. In fact, we would naively expect that the results for the reduced temperatures agree at (very) high temperatures where the quark degrees of freedom are parametrically suppressed.

In the following we show how our prescription (13) can be used to amend PNJL/PQM model studies. More precisely, we use this prescription to improve the potentials for the Polyakov loop entering these models. Alternatively to our procedure outlined in the subsequent

sections, we could also directly use the Polyakov-loop potentials obtained from our functional RG approach in a PNJL/PQM model study to get even closer to the full QCD study in Refs. [4, 5, 55]. For first studies in this direction, we refer the reader to Refs. [9, 10] where the ground state of the nonperturbative Polyakov-loop potential has been used to study the relation of confinement and chiral symmetry breaking.

III. POLYAKOV-QUARK-MESON MODEL

A. PQM model with 2+1 quark flavours

The particle content of the PQM model with 2+1 flavours are the constituent quarks minimally coupled to gauge fields, and coupled to mesons via a Yukawa-type term. The coupling to the mesons generates the masses of the quarks because the mesonic potential contains spontaneous and explicit chiral symmetry breaking. The action of the PQM model with 2+1 flavours includes kinetic terms for the dynamical low-energy degrees of freedom, quarks and mesons. The quarks are minimally coupled to a background gauge field $\langle A_0 \rangle$ as discussed in Sec. II which can be rewritten in terms of a coupling to the Polyakov loop background, $\Phi[\langle A_0 \rangle]$. The kinetic part of the model is complemented by the effective potential as a function of the order parameters and thermodynamic control parameters. In the present work we restrict ourselves to isospin symmetric matter, and do not distinguish between the up and down quark sectors. Hence, the order parameters of chiral symmetry are the light or nonstrange condensate σ and the strange chiral condensate σ_s and the pion expectation values vanish $\vec{\pi} = 0$, e.g. Refs. [25, 32]. Additionally the pure glue sector in Eq. (1), Fig. 1 leads to an effective potential of the Polyakov loop $\Phi[\langle A_0 \rangle]$. In summary, the effective potential of the model reads

$$\Omega(\sigma, \sigma_s, \Phi, \bar{\Phi}; T, \mu_f) = U(\sigma, \sigma_s) + \mathcal{U}(\Phi, \bar{\Phi}; T) + \Omega_{\text{q}\bar{\text{q}}}(\sigma, \sigma_s, \Phi, \bar{\Phi}; T, \mu_f), \quad (14)$$

where $\bar{\Phi}$ is the conjugate of Φ . The mesonic order-parameter potential for chiral symmetry breaking can be written as follows [25, 32]

$$U(\sigma, \sigma_s) = \frac{m^2}{2}(\sigma^2 + \sigma_s^2) + \frac{\lambda_1}{2}\sigma^2\sigma_s^2 + \frac{1}{8}(2\lambda_1 + \lambda_2)\sigma^4 + \frac{1}{8}(2\lambda_1 + 2\lambda_2)\sigma_s^4 - \frac{c}{2\sqrt{2}}\sigma^2\sigma_s - h\sigma - h_s\sigma_s. \quad (15)$$

Hence, the mesonic sector has six parameters that are the coupling constants m^2 , λ_1 , λ_2 and c and the explicit chiral symmetry breaking terms h and h_s . They are adjusted to the pion and kaon decay constants f_π and f_K and the meson masses of the scalar and pseudoscalar octet, namely m_π , m_K , $m_\eta^2 + m_{\eta'}^2$ and m_σ .

TABLE II. Values of constants to which the parameters of the mesonic potential are adjusted to, according to Ref. [81] and value of the constituent quark mass of the light (up and down) quarks that we use to fix the quark-meson Yukawa coupling in Eq. (18).

Constant	f_π	f_K	m_π	m_K	m_η	$m_{\eta'}$	m_σ	m_l
Value [MeV]	92	110	138	495	548	958	400-600	300

The mass of the sigma meson is not exactly known. Within our model the sigma meson is identified with the experimentally measured resonance $f_0(500)$ with mass $m_{f_0} = (400 - 550)$ MeV [81]. We will discuss the dependence of our results on this uncertainty. Once this set of masses and decay constants is given, the model parameters are defined. For their explicit derivation we refer to Refs. [25, 32]. The values of the constants we use to calculate these parameters are listed in Table II.

The last term of Eq. (14) represents the constituent quark sector and derives from the QCD flow equation (1), Fig. 1 within a 1-loop approximation to the quark loop. It includes the coupling to the Polyakov-loop variable $\Phi[\langle A_0 \rangle]$ and the mesons

$$\Omega_{\text{q}\bar{\text{q}}}(\sigma, \sigma_s, \Phi, \bar{\Phi}; T, \mu_f) = -2T \sum_{f=u,d,s} \int \frac{d^3p}{(2\pi)^3} \times \left\{ \ln \left[1 + 3 \left(\Phi + \bar{\Phi} e^{-(E_f - \mu_f)/T} \right) \times e^{-(E_f - \mu_f)/T} + e^{-3(E_f - \mu_f)/T} \right] + \ln \left[1 + 3 \left(\bar{\Phi} + \Phi e^{-(E_f + \mu_f)/T} \right) \times e^{-(E_f - \mu_f)/T} + e^{-3(E_f + \mu_f)/T} \right] \right\}. \quad (16)$$

The dispersion relation of the quarks,

$$E_f = \sqrt{k^2 + m_f^2}, \quad (17)$$

ouples the chiral condensates to the Polyakov-loop variables since the constituent light and strange quark masses are, respectively,

$$m_l = \frac{g}{2}\sigma \quad \text{and} \quad m_s = \frac{g}{\sqrt{2}}\sigma_s. \quad (18)$$

The Yukawa coupling, g , in Eq. (18) between quarks and (pseudo-)scalar mesons is fixed by choosing the constituent mass of the light quarks to be $m_l = 300$ MeV, which results in $m_s \simeq 417$ MeV for the constituent strange quarks.

One can combine nonstrange or light and strange condensate to what is called the subtracted condensate

$$\Delta_{l,s} = \frac{\sigma - \frac{h}{h_s}\sigma_s}{\sigma - \frac{h}{h_s}\sigma_s} \Big|_{T=0}. \quad (19)$$

This quantity is better accessible in lattice simulations than the condensates themselves and hence will be used for the comparison of the behaviour of the chiral sector in the PQM model with lattice calculations.

It can be easily inferred from the FRG-setting discussed in Sec. II that the effective potential detailed above has to change under a variation of the physical UV-scale Λ of the low-energy model. This follows from the fact that Λ also plays the rôle of an IR scale, up to which QCD fluctuations are integrated out, see Sec. II. In an FRG-setting the Λ -dependence can be directly computed from the flow and follows from the invariance of the effective action at vanishing cutoff scale under a variation of Λ , see the reviews [5, 27, 52–54, 77, 78, 82–84]. In the model setup this well-known fact is related to the so-called vacuum (or sea) contribution to the effective potential, see Ref. [85]. Its origin in the FRG-setting makes clear that it already includes part of the quantum fluctuations related to the UV-scale Λ . Consequently we expect significant contributions in particular for larger chemical potential, large mass scales and higher temperature. The impact on the effective potential in the PQM model is discussed in more detail in Ref. [11]. In the present work it is a subleading effect as we only consider vanishing densities and adopt low values for the mass of the σ -meson.

B. Polyakov-loop potential

The Polyakov-loop potential $\mathcal{U}(\Phi, \bar{\Phi}; T)$ simply is the pure glue potential $V_{\text{glue}}[\langle A_0 \rangle]$ defined in Eq. (8). However, in the standard approach to Polyakov-loop extended models this potential is usually modelled in the following way: The functional form for the potential contains all terms invariant under Z_3 transformations up to quartic order in the Polyakov loop (see e.g. Refs. [39, 40, 42, 44, 46]). One possible parametrisation of the Polyakov-loop potential is the polynomial parametrisation of Refs. [40, 44]. Reference [40] used a different definition of the coefficients than Ref. [44]. A simple calculation allows the translation from one set of coefficients to the other, see Ref. [50].

$$\frac{\mathcal{U}_{\text{poly}}(\Phi, \bar{\Phi}, t)}{T^4} = -\frac{b_2(t)}{2} \bar{\Phi} \Phi - \frac{b_3}{6} (\Phi^3 + \bar{\Phi}^3) + \frac{b_4}{4} (\bar{\Phi} \Phi)^2, \quad (20)$$

with the temperature-dependent coefficient b_2 defined as

$$b_2(t) = a_0 + \frac{a_1}{1+t} + \frac{a_2}{(1+t)^2} + \frac{a_3}{(1+t)^3}. \quad (21)$$

Another possible parametrisation of the Polyakov-loop potential of Ref. [46] contains a logarithmic term that restricts the Polyakov-loop expectation value to be smaller than one,

TABLE III. Parameters of the gauge potential parametrisations for fits to the lattice Yang-Mills simulations [86, 87].

	a_0	a_1	a_2	a_3	b_3	b_4
Poly-I [40]	1.53	0.96	-2.3	-2.85	13.34	14.88
Poly-II [44]	6.75	-1.95	2.625	-7.44	0.75	7.5
	A_0	A_1	A_2	B_3		
Log [46]	3.51	-2.47	15.2	-1.75		

$$\frac{\mathcal{U}_{\text{log}}(\Phi, \bar{\Phi}, t)}{T^4} = -\frac{A(t)}{2} \bar{\Phi} \Phi + B(t) \times \ln \left[1 - 6\bar{\Phi} \Phi + 4(\Phi^3 + \bar{\Phi}^3) - 3(\bar{\Phi} \Phi)^2 \right], \quad (22)$$

where both coefficients are temperature dependent,

$$A(t) = A_0 + \frac{A_1}{1+t} + \frac{A_2}{(1+t)^2}, \quad (23)$$

$$B(t) = \frac{B_3}{(1+t)^3}. \quad (24)$$

The parameters of the model potential are then determined with the help of Yang-Mills lattice data [86, 87] for the Polyakov-loop expectation value $\langle \Phi \rangle$, that is the location of the absolute minimum, and the thermodynamics, that is the value of the potential at the minimum. They are listed in Table III.

To compare the different parametrisations and parameter sets and for the later discussion of their impact we show in Figs. 8 and 9 the location of the minima of the potential and the normalised trace anomaly. We see that, first, the logarithmic parametrisation is in best agreement with the lattice data, second, the Poly-I potential features the strongest phase transition, third, the Poly-II potential leads to a relatively weak first-order transition and shows an offset of the peak of the trace anomaly compared to the other two potentials and the lattice data.

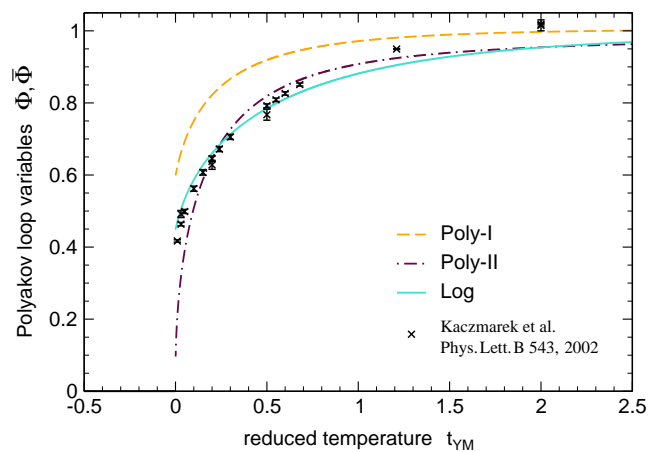


FIG. 8. Polyakov loop as a function of the reduced temperature in the pure-gauge sector for the different parametrisations and parameter sets of Table III, compared to corresponding lattice results taken from Ref. [87].

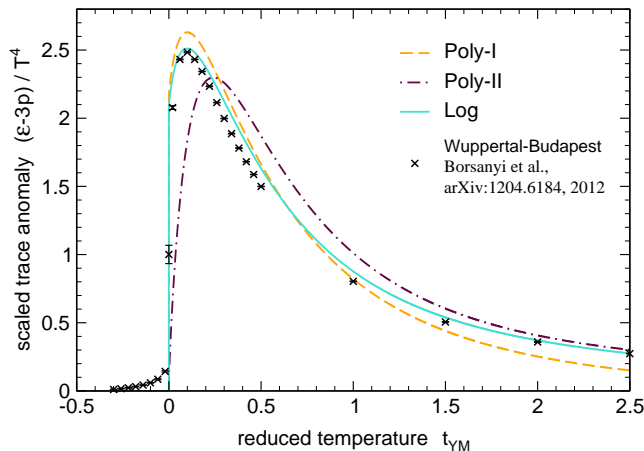


FIG. 9. Scaled trace anomaly as a function of the reduced temperature in the pure-gauge sector for the different parametrisations and parameter sets of Table III, compared to corresponding lattice results taken from Ref. [88].

The different description of the strength of the phase transition shows a significant impact on the surface tension in the PQM model at finite density [50, 89].

The construction of the Polyakov-loop potential \mathcal{U} entails that it models the pure gauge potential $\mathcal{U}_{\text{YM}}(t_{\text{YM}})/T_{\text{YM}}^4$ in terms of the variable $\langle\Phi\rangle$. It describes successfully the first order phase transition of SU(3) Yang-Mills theory. The critical temperature of the Polyakov-loop potential entering the reduced temperature is accordingly that of pure gauge theory, $T_{\text{cr}}^{\text{YM}} = 270$ MeV.

We conclude that the use of the model potentials \mathcal{U} incorporates several approximations and deficiencies: Firstly, a Yang-Mills potential is used instead of the glue potential. Secondly, it only models the Polyakov-loop potential in Yang-Mills theory by using the location of its absolute minimum and the value at the minimum. Below T_c this basically provides no information about the potential. Thirdly, the potential has to be known as a function of $\Phi[\langle A_0 \rangle]$ as the coupling to the matter sector is described in this variable. Strictly speaking, $\Phi[\langle A_0 \rangle] \approx \langle\Phi\rangle$ is only valid in the Gaussian approximation, in general we have $\Phi[\langle A_0 \rangle] \geq \langle\Phi\rangle$ up to renormalisation issues, see Refs. [16, 17].

In the present work we resolve the first approximation by using the relation between pure gauge and glue effective potential (13). This allows us to convert the Yang-Mills potential \mathcal{U}_{YM} for the Polyakov loop to a glue potential of full QCD,

$$\frac{\mathcal{U}_{\text{glue}}}{T^4}(\Phi, \bar{\Phi}, t_{\text{glue}}) = \frac{\mathcal{U}_{\text{YM}}}{T_{\text{YM}}^4}(\Phi, \bar{\Phi}, t_{\text{YM}}(t_{\text{glue}})), \quad (25)$$

with $t_{\text{YM}}(t_{\text{glue}})$ in Eq. (13). The absolute temperature scale is then determined by the value of the transition temperature (12). The resolution of the other two approximations will be discussed elsewhere.

IV. RESULTS AND DISCUSSION

Given the temperature T and the quark chemical potentials μ_f , the effective potential (14) is given as a function of the four order-parameters σ , σ_s , Φ and $\bar{\Phi}$. In equilibrium, the expectation values of the order parameters are given by extremising the effective potential

$$\frac{\partial\Omega}{\partial\sigma} = \frac{\partial\Omega}{\partial\sigma_s} = \frac{\partial\Omega}{\partial\Phi} = \frac{\partial\Omega}{\partial\bar{\Phi}} = 0. \quad (26)$$

For vanishing density the EoMs in Eq. (26), with the constraint $\Phi = \bar{\Phi}$, are given by a minimum of the effective potential. In contradistinction, for nonvanishing density, with $\Phi \neq \bar{\Phi}$ the solution of Eqs. (26) is only a saddle point, see the discussions in Refs. [6, 50, 90].

In this work we compare the solutions of the equations of motion (26) using for the Polyakov-loop potential the pure YM potential and the enhancement to a glue potential (25) by the relation (13).

The lattice results we compare our results to are the continuum extrapolations of Refs. [91, 92] and those of the HotQCD collaboration using the HISQ action and temporal lattice extent $N_\tau = 12$ (dots) and $N_\tau = 8$ (squares) of Refs. [93, 94], both with physical quark masses.

To investigate the improvement of the Polyakov-loop potential by Eqs. (25) and (13) we first show results with the combination of glue critical temperature, mass of the sigma meson and parametrisation of the Polyakov-loop potential that reproduces best the lattice results. Afterwards, we discuss the dependence of our results on the uncertainties of these parameters.

A. Improved Polyakov-loop potential

To compare the results of the PQM model using the Yang-Mills Polyakov-loop potential and the quark-improved Polyakov-loop potential we first have to choose a canonical setting for the free parameters and uncertainties that are the critical temperature and the parametrisation of the Polyakov-loop potential as well as the mass of the σ -meson.

The logarithmic parametrisation of the Polyakov-loop potential (22) with the parameters of Ref. [46] is in best agreement with the expectation value of the Polyakov loop and the equation of state of Yang-Mills theory as can be seen in Figs. 8 and 9. Therefore, we use this parametrisation for the following discussion. Furthermore, we take a medium value for the mass of the sigma meson of $m_\sigma = 500$ MeV. To adjust the critical temperature of the glue effective potential in full QCD we want to bring our model in agreement with lattice results of the normalised pressure p/T^4 since the pressure is directly related to basic quantities in lattice simulations (the free energy) and model studies (the minimum of the potential). Figure 10 shows that with $T_{\text{cr}}^{\text{glue}} = 210$ MeV we find

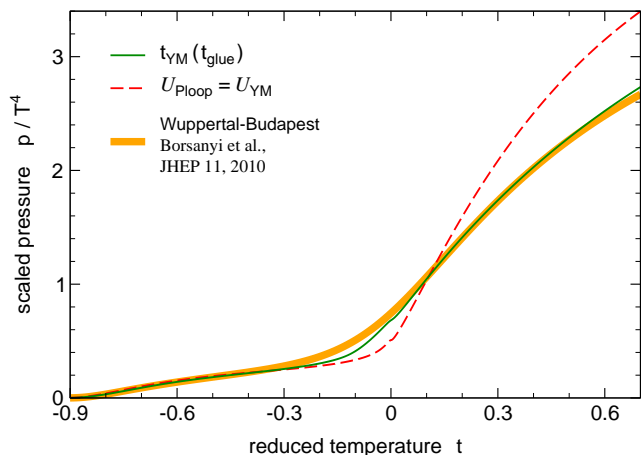


FIG. 10. Scaled pressure p/T^4 as a function of temperature at $\mu_f = 0$. The red dashed line is the result using as Polyakov-loop potential the pure Yang-Mills potential, the full green line is the case for the improvement to the glue potential. The orange band is the fit to the continuum extrapolation of the lattice results of Ref. [92].

a normalised pressure p/T^4 that is in very good agreement with the continuum extrapolated lattice results of Ref. [92].

Now that we have fixed all uncertainties we can investigate how the results evolve when we amend the pure Yang-Mills Polyakov-loop potential to a glue potential (25) by the relation (13). In Fig. 10 we see that the enhancement of the Polyakov-loop potential smoothes the phase transition significantly bringing the effective model in close agreement with lattice and functional calculations. This agreement holds in the low as well as in the high temperature phase. To achieve this agreement in the phase where chiral symmetry is broken we took into account the contribution of thermal pions.

The critical temperature of the glue potential $T_{\text{cr}}^{\text{glue}} = 210$ MeV for which we find the best agreement with the lattice calculation is larger than the estimate for 2+1 quark flavours of Ref. [6]. But this estimate of $T_{\text{cr}}^{\text{glue}}(2+1) = 182$ MeV is only a lower limit as outlined in Sec. II when discussing Eq. (12). We find comparable curves for the combinations $(m_\sigma = 400$ MeV, $T_{\text{cr}}^{\text{glue}} = 180$ MeV) and $(m_\sigma = 600$ MeV, $T_{\text{cr}}^{\text{glue}} = 250$ MeV). We will discuss the impact of the critical temperature of the Polyakov-loop potential and of the mass of the σ -meson in detail in the following sections.

To complete the discussion of the pressure shown in Fig. 10 let us note that the result of the PQM model with the quark-improved Polyakov-loop potential still shows a transition that is marginally steeper than that on the lattice. A quantitative probe of this slight deviation is the trace anomaly or interaction measure which tests not only the free energy or minimum of the potential but contains as well information about their temperature derivative. In Fig. 11 we compare results for the normalised trace anomaly $(\epsilon - 3p)/T^4$. Even though the agreement

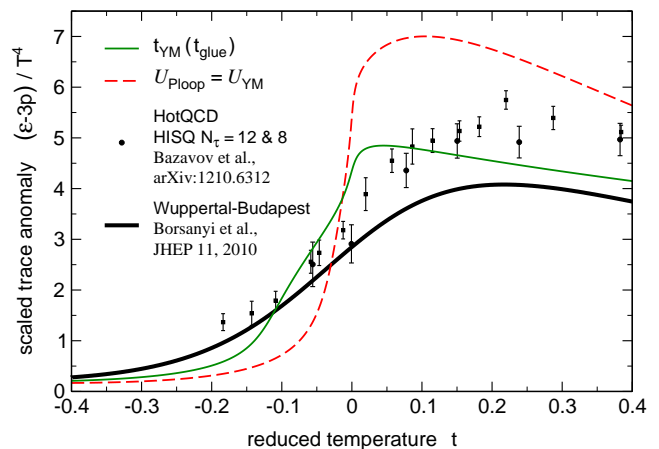


FIG. 11. Scaled trace anomaly $(\epsilon - 3p)/T^4$ as function of temperature at $\mu_f = 0$. The red dashed line is the result using as Polyakov-loop potential the pure Yang-Mills potential, the full green line when the improvement to the glue potential by the adjustment from functional calculations is taken into account. The black band is the fit to the continuum extrapolation of the lattice results of Ref. [92] and the data points lattice results of the HotQCD collaboration [94].

of the normalised pressure of the effective model using the improved glue potential and the lattice calculation is remarkably close the slight differences get more visible in the trace anomaly. The amplitude is in good agreement with lattice results, nevertheless the transition in the effective model is still steeper than in lattice calculations. However, the calculations done here within a basic effective model neglect contributions from correlations. Taking those into account smoothes the phase transition, as is shown e.g. in Refs. [8, 49] which will lead to a better agreement.

Anyhow, one sees in the interaction measure that the improved glue potential smoothes the transition compared to the standard calculation with the Yang-Mills Polyakov-loop potential. So the emergence of the quark degrees of freedom happens in a larger temperature interval and its amplitude is in better agreement with lattice results.

After this analysis of thermodynamic quantities, let us now analyse the evolution of the order parameters that are the Polyakov loop for deconfinement and the subtracted chiral condensate (19) for chiral symmetry restoration.

The biggest discrepancy between Polyakov-loop extended effective models and lattice results for full QCD is seen in the Polyakov-loop expectation value [48]. The lattice data shows a smoother transition with significant smaller values. This can be seen in Fig. 12 and holds as well when the quark-improved Polyakov-loop potential is applied. Including contributions of fluctuations to the model will certainly reduce this large offset to the lattice data. However, a part of the discrepancy originates in the inherent approximations which are still present: the

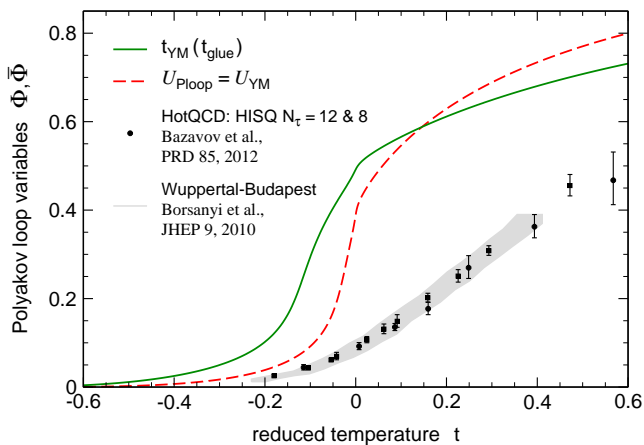


FIG. 12. The Polyakov-loop expectation value Φ as function of temperature at $\mu_f = 0$. The red dashed line is the result using as the Polyakov-loop potential the pure Yang-Mills potential, the full green line when the improvement to the glue potential by the adjustment from functional calculations is taken into account. The grey band is the continuum extrapolation of the lattice results of Ref. [91] and the data points lattice results of Ref. [93].

derivation of the PQM model from QCD entails that the Polyakov-loop variable in the quark loop is $\Phi[\langle A_0 \rangle]$ and not $\langle \Phi \rangle$ as used in the Polyakov-loop-model potentials \mathcal{U} . This mismatch can be resolved by using the QCD glue potential V_{glue} as defined in Eq. (8). Then the model is fully consistent with its QCD counterpart defined by the flow equation (1). The Polyakov loop observable accessible in such a continuum approach to full QCD is $\Phi[\langle A_0 \rangle]$ and not $\langle \Phi \rangle$ computed on the lattice. The former observable has been computed in Ref. [4] within QCD-flows for two-flavour QCD in the chiral limit. It shows a rather smooth transition but cannot be directly compared with present lattice data. On the lattice, the chiral limit is not yet accessible. In any case, the two observables are different and mapping them into each other is an interesting open issue.

One sees in Fig 12 that by applying the improved glue potential, the Polyakov loop is shifted differently in the two phases, as anticipated in Figs. 5 and 7 and Eq. (13). So, the Polyakov-loop variables are shifted to higher expectation values in the confined phase and to lower values in the deconfined phase. This shift in the respective phases is what leads to a overall smoother transition, not only of the Polyakov-loop expectation value. The evolution of the Polyakov loop when the quark-improved potential is considered has the advantage that the Polyakov-loop variables are shifted to a value of ~ 0.5 at the transition which is a reasonable criterion to define the transition between the confined phase and the quark gluon plasma in case of a crossover.

The adjustment of the Polyakov-loop potential from the pure gauge potential to the glue potential in full QCD does not only affect the Polyakov-loop expectation value

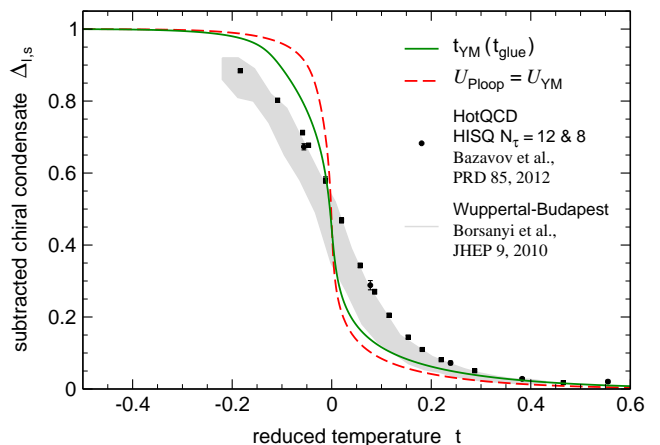


FIG. 13. The subtracted chiral condensate $\Delta_{1,s}$ as a function of temperature at $\mu_f = 0$. The red dashed line is the result using as Polyakov-loop potential the pure Yang-Mills potential, the full green line when the improvement to the glue potential by the adjustment from functional calculations is adopted. The grey band is the continuum extrapolation of the lattice results of Ref. [91] and the data points lattice results of Ref. [93], see also Ref. [95].

TABLE IV. Pseudocritical temperatures for the crossover phase transition at $\mu_f = 0$. They are determined by the peaks in the temperature derivatives of the subtracted condensate $\Delta_{1,s}$.

	\mathcal{U}_{YM}	$\mathcal{U}_{\text{glue}}$	lattice Wuppertal-Budapest [91]	lattice HotQCD $N_\tau = 12 \& 8$ [93]
T_c [MeV]	168	158	157	159 & 163

but also quarks and mesonic degrees of freedom because of the nontrivial coupling to the gauge field. Therefore, we show in Fig. 13 how the subtracted chiral condensate evolves with increasing temperature for vanishing density. The result of the PQM model using as Polyakov-loop potential the pure gauge potential and the improvement to the glue potential from functional calculations show both a steeper decrease in the transition region than the lattice calculations. Nevertheless, the adjustment of the gauge potential to the glue potential leads to a smoother chiral transition and to an improvement towards the result of lattice calculations.

In the previous and following figures the abscissae are in units of the reduced temperature of full QCD $t = (T - T_c)/T_c$. To have a unique criterion for lattice and model calculations we determine the pseudocritical temperature T_c of the crossover transition by the peak of the susceptibility of the subtracted chiral condensate. Table IV summarises the hereby defined pseudocritical temperatures for the lattice calculations and the model calculations with the Yang-Mills and improved glue Polyakov-loop potential. We see that applying the quark-improved Polyakov-loop potential leads to a reduction of the pseudocritical temperature. With $T_c = 158$ MeV we get a

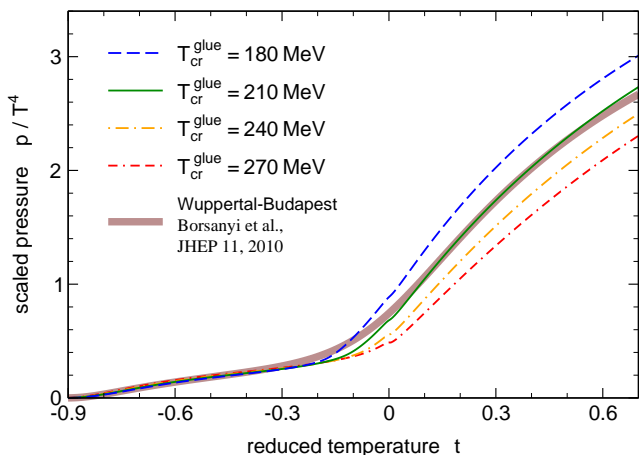


FIG. 14. Scaled pressure p/T^4 as a function of temperature at $\mu_f = 0$ with the adjustment to the glue potential for four different glue critical temperatures. The brown band is the fit to the continuum extrapolation of the lattice results of Ref. [92].

result that is in very good agreement with the best lattice calculations. That is another important ingredient to find the nice agreement of our results for the equation of state and order parameters.

We conclude that adjusting the gauge potential to the glue potential in full QCD by applying Eqs. (25) and (13) improves the description of the chiral and (de)confinement phase transition with effective models.

B. Dependence on the glue critical temperature

In the last section we have showed that replacing the pure Yang-Mills Polyakov-loop potential by the quark-improved potential from functional calculations smoothes the phase transition significantly and brings it to closer agreement with lattice and functional calculations. Now, we will investigate the dependence of our results on the critical temperature of the glue potential $T_{\text{cr}}^{\text{glue}}$. It is not yet uniquely defined so that we consider it as a parameter. According to the discussion in Sec. II around Eq. (12) we expect it to be in the interval (180 – 270) MeV. For this investigation we use again the logarithmic parametrisation of the Polyakov-loop potential and a medium sigma meson mass of $m_\sigma = 500$ MeV. For purpose of illustration we omit in the following figures to show the results with the Yang-Mills Polyakov-loop potential but choose the same range of the ordinates as in the previous section to give an estimate of the reduction due to the application of the quark-improved Polyakov-loop potential. We show the results with both potentials in the same plots elsewhere [96].

Let us start again with the discussion of the normalised pressure p/T^4 . We see in Fig. 14 that the pressure rises already at smaller relative temperatures and that it shows a slightly steeper increase when the critical tem-

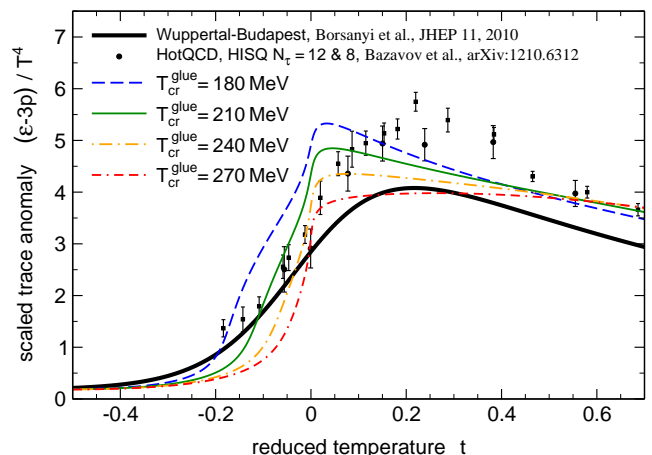


FIG. 15. Scaled trace anomaly $(\epsilon - 3p)/T^4$ as function of temperature at $\mu_f = 0$ with the adjustment to the glue potential for four different glue critical temperatures. The black band is the fit to the continuum extrapolation of the lattice results of Ref. [92] and the data points lattice results of the HotQCD collaboration [94].

TABLE V. Pseudocritical temperatures for the crossover transition at $\mu_f = 0$ for different critical temperatures of the glue potential. They are determined by the peaks of the chiral susceptibility $\partial\Delta_{1,s}/\partial T$.

$T_{\text{cr}}^{\text{glue}}$ [MeV]	180	210	240	270
T_c [MeV]	152	158	164	171

perature of the Polyakov-loop potential is lowered. Together with the respective pseudocritical temperatures that are summarised in Table V the best agreement with lattice results shows the curve with a critical temperature of the glue potential of $T_{\text{cr}}^{\text{glue}} = 210$ MeV. As discussed in the previous section the pseudocritical temperature of $T_c = 158$ MeV for $T_{\text{cr}}^{\text{glue}} = 210$ MeV is in accordance with the lattice result. But also the value for $T_{\text{cr}}^{\text{glue}} = 180$ MeV of $T_c = 152$ MeV is on the lower end of the transition region of lattice calculations [91]. As addressed already in the previous section including fluctuations to the model smoothes the phase transition additionally [8, 49] and slightly increases the transition temperature as shows e.g. a comparison of Refs. [6] and [8]. So we can expect that taking into account fluctuations of quarks and mesons would decrease the transition temperature of the glue potential for which we find best agreement with the lattice calculation towards the 2+1 flavour estimate of Ref. [6]. We will address the quantitative analysis in a future work.

For the detailed investigation of the steepness of the transition in dependence of the critical temperature of the improved glue potential we show in Fig. 15 the normalised trace anomaly or interaction measure. We see that using our adjustment of the Polyakov-loop potential towards the glue potential of full QCD the overall ampli-

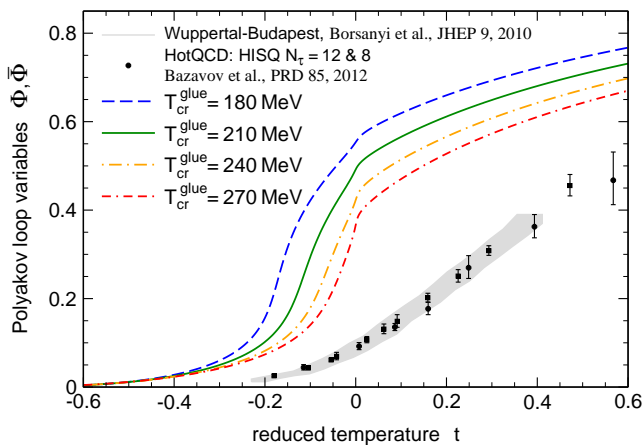


FIG. 16. The Polyakov-loop expectation value Φ as function of temperature at $\mu_f = 0$ with the adjustment to the glue potential for four different glue critical temperatures. The grey band is the continuum extrapolation of the lattice results of Ref. [91] and the data points lattice results of Ref. [93].

tude is in good agreement with lattice calculations. Like anticipated in the discussion of the pressure the steepness of the transition increases when the critical temperature of the Polyakov-loop potential is lowered. Furthermore, the transition region broadens towards lower relative temperatures with decreasing transition temperature of the gauge potential.

An important aspect that we see in Fig. 15 is that the slope of the trace anomaly becomes smaller and unnatural above T_c for large critical temperatures of the Polyakov-loop potential. This behaviour has two reasons. First, the pseudocritical temperature is shifted towards the lower end of the transition region for larger transition temperatures of the glue potential, so that the transition region extends well above the pseudocritical temperature. So the emergence of the quark degrees of freedom holds on above T_c and avoids a decrease of the interaction measure. Second, the saturation scale of our adjustment between pure YM Polyakov-loop potential and quark-improved glue potential, i.e., the upper limit of validity of Eq. (13), is closer to the transition scale for larger critical temperatures of the Polyakov-loop potential, see Table V.

In Fig. 16 we show the dependence of the evolution of the Polyakov-loop expectation values on the critical temperature of the glue Polyakov-loop potential. The magnitude of the transition increases when the transition temperature of the Polyakov-loop potential is lowered and the transition regions is shifted towards smaller relative temperatures. So the onset of deconfinement shifts towards the lower end of the transition region with decreasing critical temperature of the Polyakov-loop potential. This is a natural consequence, as decreasing the scale of the Polyakov-loop potential leads to a relative shift of the glue part towards a lower scale in the full theory. Overall, the value of the Polyakov-loop variables shows a large

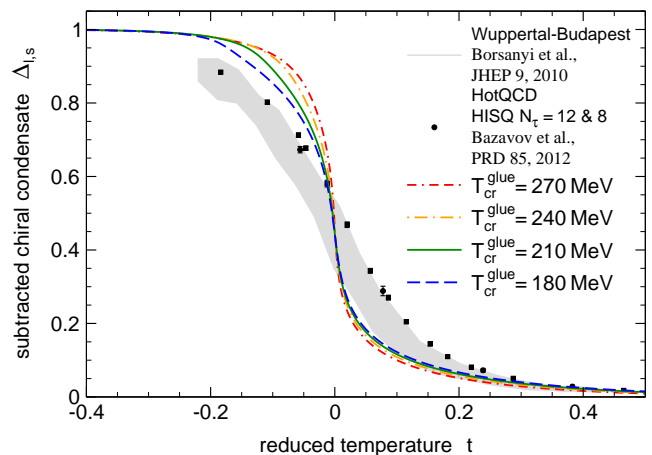


FIG. 17. The subtracted chiral condensate $\Delta_{1,s}$ as a function of temperature at $\mu_f = 0$ with the adjustment to the glue potential for four different glue critical temperatures. The grey band is the continuum extrapolation of the lattice results of Ref. [91] and the data points lattice results of Ref. [93].

sensitivity on the critical temperature of the Polyakov-loop potential but the general discrepancy to the lattice results is too large for any constraints.

Due to the nontrivial coupling between Polyakov loop, quarks and mesons, the onset of deconfinement at lower temperatures with decreasing critical temperatures of the Polyakov-loop potential shows its impact also in the order parameter for chiral symmetry, the subtracted chiral condensate which is plotted in Fig. 17. It deviates at relative smaller temperatures from its vacuum value when the transition temperature of the Polyakov-loop potential is lowered. This effect gets enhanced due to the simultaneous lowering of the pseudocritical temperature. Apart from that, the chiral condensate shows only a very mild dependence on the transition temperature of the glue potential.

C. Dependence on the parametrisation

The second uncertainty in the gauge sector of PNJL & PQM models besides the transition temperature of the Polyakov-loop potential is its form of parametrisation. We demonstrated in Figs. 8 and 9 that the different forms and parameter sets show a significant difference already in pure YM theory. Ideally, the Polyakov-loop potential of full QCD from first principal calculations should be applied. Since this is not yet directly applicable one can at least consider the uncertainty that comes along with the different parametrisations and parameter sets.

For the comparison of the different parametrisations of the Polyakov-loop potential we choose a sigma meson mass of 500 MeV and a transition temperature of the Polyakov-loop potential of 210 MeV. For better readability of the plots we omit in the following figures the results with the pure YM Polyakov-loop potential and

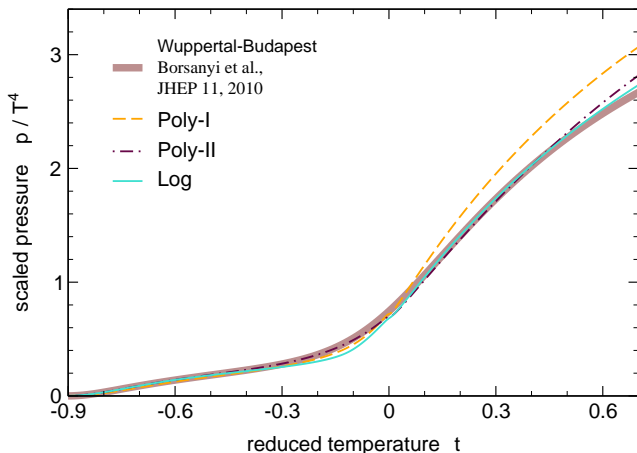


FIG. 18. Scaled pressure p/T^4 as a function of temperature at $\mu_f = 0$ with the adjustment to the glue potential for three different parametrisations and parameter sets of the Polyakov-loop potential. The orange band is the fit to the continuum extrapolation of the lattice results of Ref. [92].

choose the same range of the ordinates as in Sec. IV A to give an estimate of the reduction due to the application of the quark-improved Polyakov-loop potential. The figures with the results with both potentials will be presented in Ref. [96].

The normalised pressure (Fig. 18) shows the steepest rise in the transition region for the polynomial parametrisation with the parameters of Ref. [40] (Poly-I potential). This is in accord with the description of pure Yang-Mills theory discussed in Sec. III B. Overall, the difference in the results for the scaled pressure for the different parametrisations is not large around the transition region.

As seen before, the differences are more pronounced for the trace anomaly or interaction measure (Fig. 19). The slopes of the curves are similar for the Poly-I and logarithmic parametrisation but with a larger amplitude in the case of the Poly-I potential. This originates from the description of pure Yang-Mills theory as seen in Fig. 9. The normalised trace anomaly with the Poly-II parametrisation of Ref. [44] is nearly constant above the transition temperature. This is a feature of the offset of the maximum of the trace anomaly in Yang-Mills theory seen in Fig. 9. This offset is also seen in calculations of full QCD with the Yang-Mills Polyakov-loop potential [48]. The overall reduction of the amplitude in the transition region for the improved glue potential leads to the behaviour seen in Fig. 19.

The evolution of the Polyakov-loop variables shown in Fig. 20 reveals that the onset of the transition in the confined phase is the steepest with the logarithmic potential. The Poly-II parametrisation leads to the smoothest evolution of the Polyakov loop below the pseudocritical temperature. Note that we normalised the Polyakov-loop expectation value shown in Fig. 20 for the calculations with the polynomial parametrisation such that it tends

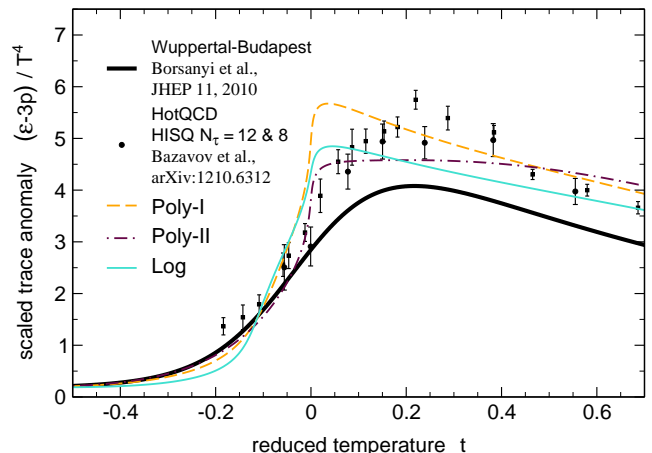


FIG. 19. Scaled trace anomaly $(\epsilon - 3p)/T^4$ as a function of temperature at $\mu_f = 0$ with the adjustment to the glue potential for three different parametrisations and parameter sets of the Polyakov-loop potential. The black band is the fit to the continuum extrapolation of the lattice results of Ref. [92] and the data points lattice results of the HotQCD collaboration [94].

towards unity at infinite temperature. Overall, the differences in the Polyakov-loop variables due to the different parametrisations are so large that it should be considered before making quantitative statements.

Nevertheless, the differences in the gauge sector due to the different parametrisations are considerably smaller in the evolution of the subtracted chiral condensate (Fig. 21). The slightly stronger transition in the gauge sector for the Poly-I potential shifts the pseudocritical temperature to a smaller value compared to the other cases as seen in Table VI.

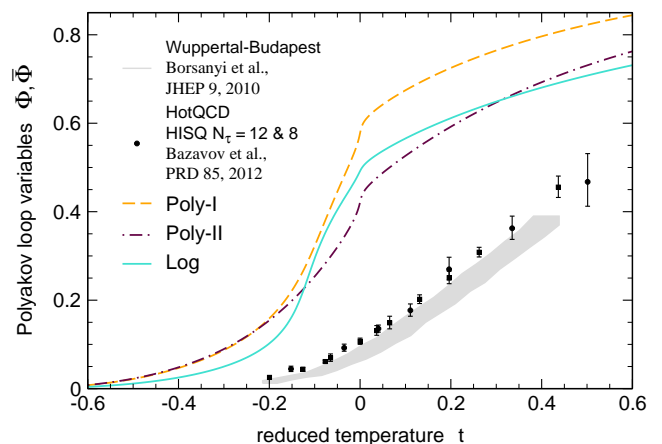


FIG. 20. The Polyakov-loop expectation value Φ as function of temperature at $\mu_f = 0$ with the adjustment to the glue potential for three different parametrisations and parameter sets of the Polyakov-loop potential. The grey band is the continuum extrapolation of the lattice results of Ref. [91] and the data points lattice results of Ref. [93].

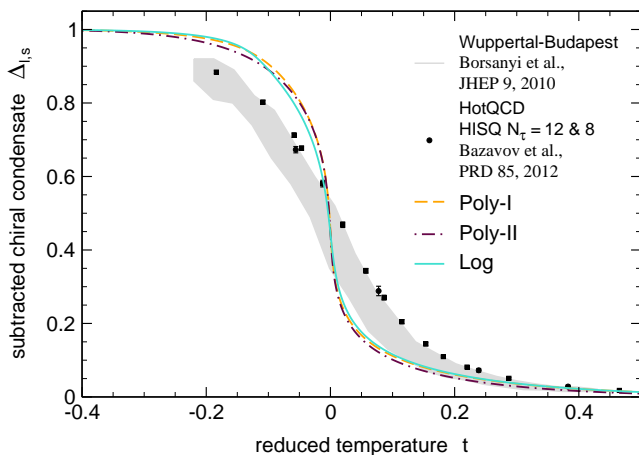


FIG. 21. The subtracted chiral condensate $\Delta_{1,s}$ as a function of temperature at $\mu_f = 0$ with the adjustment to the glue potential for three different parametrisations and parameter sets of the Polyakov-loop potential. The grey band is the continuum extrapolation of the lattice results of Ref. [91] and the data points lattice results of Ref. [93], see also Ref. [95].

TABLE VI. Pseudocritical temperatures for the crossover transition at $\mu_f = 0$ for different parametrisations and parameter sets of the Polyakov-loop potential. They are determined by the peaks of the chiral susceptibility $\partial\Delta_{1,s}/\partial T$.

	Poly-I	Poly-II	Log
T_c [MeV]	144	158	158

D. Dependence on the sigma meson mass

Usually, the chiral partner of the pion is associated with the resonance $f_0(500)$ [81]. Note however that in Ref. [97] it was demonstrated that within an extended quark-meson model that includes vector and axial-vector mesons the resonance $f_0(1370)$ was identified as the non-strange scalar quarkonium state. Within our simple quark-meson model we consider $m_\sigma = (400 - 600)$ MeV to be a reasonable parameter range.

To investigate the role of the mass of the scalar sigma meson the logarithmic parametrisation of the Polyakov-loop potential with a transition temperature of 210 MeV is used in the following.

The normalised pressure as displayed in Fig. 22 shows that the steepness of the transition is relatively independent on the mass of the σ -meson. The location of the pseudocritical temperature relative to the transition region leads to differences in the evolution. For $m_\sigma = 400$ MeV the pseudocritical temperature is small (see Table VII) and at the lower end of the transition region so that the pressure just starts to rise at T_c . The evolution for $m_\sigma = 600$ MeV is the other extreme. Here,

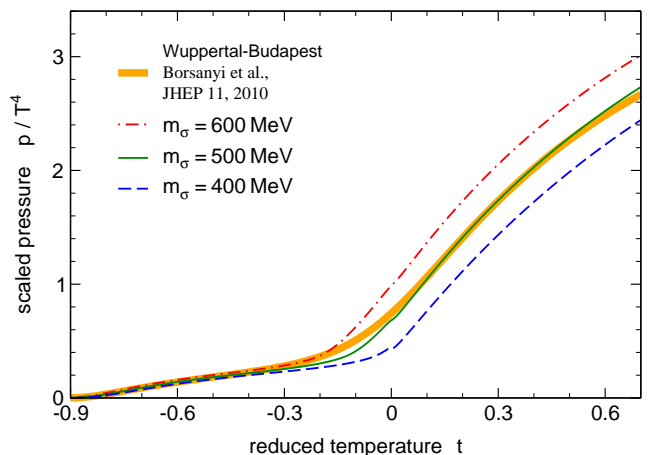


FIG. 22. Scaled pressure p/T^4 as a function of temperature at $\mu_f = 0$ with the adjustment to the glue potential for three different masses of the sigma meson. The orange band is the fit to the continuum extrapolation of the lattice results of Ref. [92].

TABLE VII. Pseudocritical temperatures for the crossover transition at $\mu_f = 0$ for different masses of the sigma meson. They are determined by the peaks in the temperature derivatives of the subtracted condensate $\Delta_{1,s}$.

m_σ [MeV]	400	500	600
T_c [MeV]	144	158	173

the scaled pressure rises already significantly below T_c since the pseudocritical temperature is just reached at the upper end of the transition region and at a relatively large absolute value as given in Table VII.

The change of the pressure for an increasing mass of the sigma meson (Fig. 22) is opposite to the case of an increasing glue critical temperature (Fig. 14). Therefore, to get agreement with the pressure of the lattice calculation for a sigma meson mass of 400 MeV one would have to choose a critical temperature of the glue potential of 180 MeV and for $m_\sigma = 600$ MeV one would require $T_{cr}^{glue} = 250$ MeV. So the lower the mass of the sigma meson, the smaller the transition temperature of the glue potential has to be in order to reproduce the lattice results. This is due to the fact that a decrease in the mass of the sigma meson lowers the scale of the chiral transition as can be seen in Table VII and Ref. [32]. So the scale of the (de)confinement transition has to decrease as well. Note that the combination of $m_\sigma = 500$ MeV and $T_{cr}^{glue} = 210$ MeV leads to a pseudocritical temperature that is equal to the one of lattice calculations.

Figure 23 shows the results of the trace anomaly for different sigma meson masses. The transition region broadens for a larger mass of the σ -meson.

The subtracted condensate is shown in Fig. 24. The larger the mass of the sigma meson, the earlier the chiral condensate deviates from its vacuum expectation value.

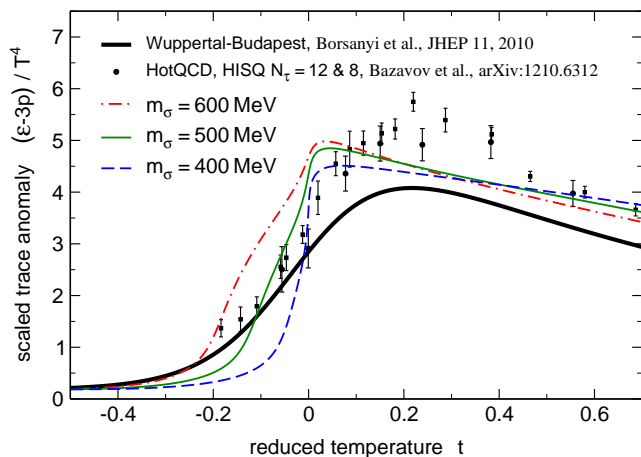


FIG. 23. Scaled trace anomaly $(\epsilon - 3p)/T^4$ as a function of temperature at $\mu_f = 0$ with the adjustment to the glue potential for three different masses of the sigma meson. The black band is the fit to the continuum extrapolation of the lattice results of Ref. [92] and the data points lattice results of the HotQCD collaboration [94].

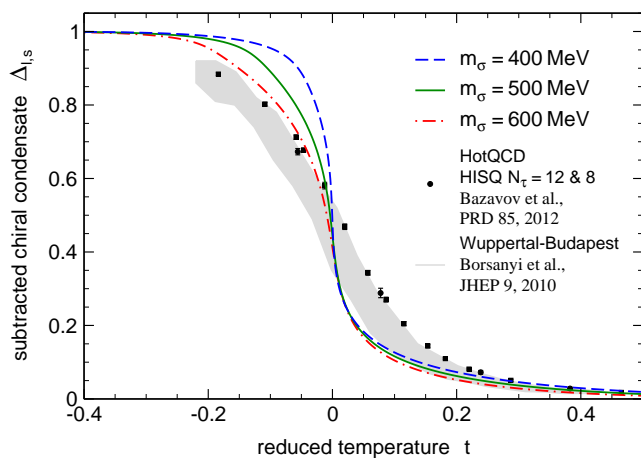


FIG. 24. The subtracted chiral condensate $\Delta_{1,s}$ as a function of temperature at $\mu_f = 0$ with the adjustment to the glue potential for three different masses of the sigma meson. The grey band is the continuum extrapolation of the lattice results of Ref. [91] and the data points lattice results of Ref. [93].

The temperature dependence of the chiral condensate becomes smoother with larger σ -meson masses.

The evolution of the Polyakov-loop variables (Fig. 25) shows that the transition regions shrinks when the mass of the sigma meson is lowered. Decreasing the glue critical temperature broadens the transition region towards lower temperatures. The pseudocritical temperatures for $m_\sigma = 400$ MeV is already smaller than the lattice result for $T_{\text{cr}}^{\text{glue}} = 210$ MeV.

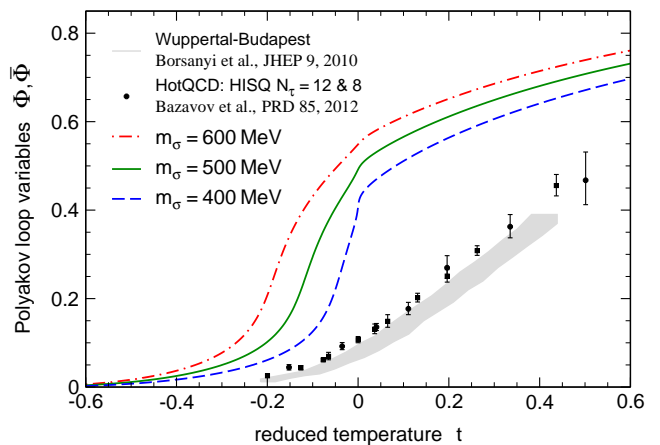


FIG. 25. The Polyakov-loop expectation value Φ as function of temperature at $\mu_f = 0$ with the adjustment to the glue potential for three different masses of the sigma meson. The grey band is the continuum extrapolation of the lattice results of Ref. [91] and the data points lattice results of Ref. [93].

V. CONCLUSIONS & OUTLOOK

In this work we have presented results for the non-perturbative Polyakov-loop potential in QCD in terms of the expectation value $\langle A_0 \rangle$. The potential $V[\langle A_0 \rangle]$ is an order-parameter potential for the deconfinement transition. It is obtained from the first-principle QCD flows in Refs. [4, 5] solely from the QCD two-point functions of the ghost and the gluon fields. In particular this computation takes into account the full backreaction of the quarks and the nonlinear coupling of the quark-gluon sector. So far, this important physics has been omitted in Polyakov-loop potentials used in PNJL/PQM models, where a Polyakov-potential is used which is generated solely from lattice Yang-Mills data for the Polyakov loop and the thermodynamic observables.

In Sec II, we have compared the glue Polyakov loop potential with that in pure Yang-Mills theory [16, 18, 19]. We have shown that the two potentials are simply related by an appropriate rescaling of the temperature, see Eq. (25). Such an approach allows to mimic the effect of the quark backreaction on the gauge sector describing the confining dynamics. Whereas the fit of the parameters of the Polyakov-loop potential to the lattice data contains only information about the minimum of the potential in the deconfined phase, our fit also adjusts the potential in the confined phase. In total this provides a simple method for improving effective low-energy models towards full QCD.

In the second part of this work, we have applied this improvement in the 2+1 flavour PQM model. Our adjustment of the temperature scale of the Polyakov-loop potentials leads to a softening of the temperature dependence of physical observables at temperatures close to the chiral and deconfinement crossover at vanishing chemical potential. As a consequence, the behaviour of

the order parameters and thermodynamic observables is in much better agreement with latest results from lattice QCD studies and first-principles functional approaches. Specifically, we find good agreement with the scaled pressure and the trace anomaly from lattice QCD simulations, even for the amplitude of the trace anomaly.

In order to test the robustness of our results, we have analysed the dependence on the parametrisation and the transition temperature of the Polyakov-loop potential as well as the σ -meson mass. We have found a parametrisation-dependence of the results, which can not be ignored in a quantitative analysis. To be more specific, we have varied the glue critical temperature and the mass of the scalar σ -meson and observed that a larger glue critical temperature has a similar effect on our results as a decrease of the mass of the σ -meson. In comparison to the computation without QCD-improved Polyakov-loop potential we find a qualitatively better agreement with the lattice data, see in particular the trace anomaly in Fig. 11. For a sigma meson mass $m_\sigma \approx 500$ MeV and a transition temperature of the glue potential of ~ 210 MeV this agreement is most pronounced.

We have also discussed the next steps for systematically improving PNJL/PQM models towards low-energy QCD. These steps include the determination of the input parameters in the chiral sector, i.e., m_σ , from the QCD flows. Furthermore, the model potentials can be upgraded by successively taking into account more infor-

mation from the full glue potential. One possibility is e.g. to work-in the correct height of the barrier and the difference of the potential at the minima in the metastable region. This has a direct impact on the steepness of both transitions. Finally the QCD potential obtained from the flow equation [4, 5] can be used directly, see also Refs. [9, 10, 74]. Moreover, matter fluctuations can be included within an extension of the present work and Ref. [11].

In conclusion, the present work offers a simple and systematic approach for improving the gauge sector of low-energy effective models towards QCD. The comparison of our results with that from lattice QCD confirms that this is important as it significantly affects the behaviour of physical observables in the crossover region.

ACKNOWLEDGMENTS

We thank L. Fister, E. S. Fraga, T. K. Herbst, B. W. Mintz and B.-J. Schaefer for discussions and collaboration on related topics. This work is supported by BMBF under grants FKZ 05P12VHCTG and 06HD7142, by ERC-AdG-290623, by the Helmholtz Alliance HA216/EMMI, by the DFG through the HGSFP, by HGS-HIRe, and by HIC for FAIR within the LOEWE program.

-
- [1] D. Boyanovsky, H. de Vega, and D. Schwarz, *Ann. Rev. Nucl. Part. Sci.* **56**, 441 (2006), arXiv:hep-ph/0602002.
 - [2] F. Weber, *Prog. Part. Nucl. Phys.* **54**, 193 (2005), arXiv:astro-ph/0407155.
 - [3] B. Muller, J. Schukraft, and B. Wyslouch, *Ann. Rev. Nucl. Part. Sci.* **62**, 361 (2012), arXiv:1202.3233 [hep-ex].
 - [4] J. Braun, L. M. Haas, F. Marhauser, and J. M. Pawłowski, *Phys. Rev. Lett.* **106**, 022002 (2011), arXiv:0908.0008 [hep-ph].
 - [5] J. M. Pawłowski, *AIP Conf. Proc.* **1343**, 75 (2011), arXiv:1012.5075 [hep-ph].
 - [6] B.-J. Schaefer, J. M. Pawłowski, and J. Wambach, *Phys. Rev. D* **76**, 074023 (2007), arXiv:0704.3234 [hep-ph].
 - [7] V. Skokov, B. Stokic, B. Friman, and K. Redlich, *Phys. Rev. C* **82**, 015206 (2010), arXiv:1004.2665 [hep-ph].
 - [8] T. K. Herbst, J. M. Pawłowski, and B.-J. Schaefer, *Phys. Lett. B* **696**, 58 (2011), arXiv:1008.0081 [hep-ph].
 - [9] J. Braun and A. Janot, *Phys. Rev. D* **84**, 114022 (2011), arXiv:1102.4841 [hep-ph].
 - [10] J. Braun and T. K. Herbst, (2012), arXiv:1205.0779 [hep-ph].
 - [11] T. K. Herbst, J. M. Pawłowski, and B.-J. Schaefer, (2013), arXiv:1302.1426 [hep-ph].
 - [12] H. Gies and J. Jaeckel, *Eur. Phys. J. C* **46**, 433 (2006), arXiv:hep-ph/0507171.
 - [13] J. Braun and H. Gies, *Phys. Lett. B* **645**, 53 (2007), arXiv:hep-ph/0512085.
 - [14] J. Braun and H. Gies, *JHEP* **0606**, 024 (2006), arXiv:hep-ph/0602226.
 - [15] J. Braun, *Eur. Phys. J. C* **64**, 459 (2009), arXiv:0810.1727 [hep-ph].
 - [16] J. Braun, H. Gies, and J. M. Pawłowski, *Phys. Lett. B* **684**, 262 (2010), arXiv:0708.2413 [hep-th].
 - [17] F. Marhauser and J. M. Pawłowski, (2008), arXiv:0812.1144 [hep-ph].
 - [18] J. Braun, A. Eichhorn, H. Gies, and J. M. Pawłowski, *Eur. Phys. J. C* **70**, 689 (2010), arXiv:1007.2619 [hep-ph].
 - [19] L. Fister and J. M. Pawłowski, (2013), arXiv:1301.4163 [hep-ph].
 - [20] K. Fukushima and C. Sasaki, (2013), arXiv:1301.6377 [hep-ph].
 - [21] M. Gell-Mann and M. Levy, *Nuovo Cim.* **16**, 705 (1960).
 - [22] D. Metzger, H. Meyer-Ortmanns, and H. Pirner, *Phys. Lett. B* **321**, 66 (1994), arXiv:hep-ph/9312252.
 - [23] J. Berges, D. Jungnickel, and C. Wetterich, *Phys. Rev. D* **59**, 034010 (1999), arXiv:hep-ph/9705474.
 - [24] B.-J. Schaefer and H.-J. Pirner, *Nucl. Phys. A* **660**, 439 (1999), arXiv:nucl-th/9903003.
 - [25] J. T. Lenaghan, D. H. Rischke, and J. Schaffner-Bielich, *Phys. Rev. D* **62**, 085008 (2000), arXiv:nucl-th/0004006.
 - [26] O. Scavenius, A. Mocsy, I. Mishustin, and D. Rischke, *Phys. Rev. C* **64**, 045202 (2001), arXiv:nucl-th/0007030.
 - [27] J. Berges, N. Tetradis, and C. Wetterich, *Phys. Rept.*

- 363**, 223 (2002), arXiv:hep-ph/0005122.
- [28] J. Braun, K. Schwenzer, and H.-J. Pirner, Phys. Rev. **D 70**, 085016 (2004), arXiv:hep-ph/0312277.
- [29] A. Mocsy, I. Mishustin, and P. Ellis, Phys. Rev. **C 70**, 015204 (2004), arXiv:nucl-th/0402070.
- [30] B.-J. Schaefer and J. Wambach, Nucl. Phys. **A 757**, 479 (2005), arXiv:nucl-th/0403039.
- [31] E. S. Bowman and J. I. Kapusta, Phys. Rev. **C 79**, 015202 (2009), arXiv:0810.0042 [nucl-th].
- [32] B.-J. Schaefer and M. Wagner, Phys. Rev. **D 79**, 014018 (2009), arXiv:0808.1491 [hep-ph].
- [33] Y. Nambu and G. Jona-Lasinio, Phys. Rev. **122**, 345 (1961).
- [34] Y. Nambu and G. Jona-Lasinio, Phys. Rev. **124**, 246 (1961).
- [35] S. Klevansky, Rev. Mod. Phys. **64**, 649 (1992).
- [36] M. Buballa, Phys. Rept. **407**, 205 (2005), arXiv:hep-ph/0402234.
- [37] P. Costa, M. Ruivo, and C. de Sousa, Phys. Rev. **D 77**, 096001 (2008), arXiv:0801.3417 [hep-ph].
- [38] P. N. Meisinger and M. C. Ogilvie, Phys. Lett. **B 379**, 163 (1996), arXiv:hep-lat/9512011.
- [39] R. D. Pisarski, Phys. Rev. **D 62**, 111501 (2000), arXiv:hep-ph/0006205.
- [40] O. Scavenius, A. Dumitru, and J. Lenaghan, Phys. Rev. **C 66**, 034903 (2002), arXiv:hep-ph/0201079.
- [41] A. Mocsy, F. Sannino, and K. Tuominen, Phys. Rev. Lett. **92**, 182302 (2004), arXiv:hep-ph/0308135.
- [42] K. Fukushima, Phys. Lett. **B 591**, 277 (2004), arXiv:hep-ph/0310121.
- [43] E. Megias, E. Ruiz Arriola, and L. Salcedo, Phys. Rev. **D 74**, 065005 (2006), arXiv:hep-ph/0412308.
- [44] C. Ratti, M. A. Thaler, and W. Weise, Phys. Rev. **D 73**, 014019 (2006), arXiv:hep-ph/0506234.
- [45] C. Sasaki, B. Friman, and K. Redlich, Phys. Rev. **D 75**, 074013 (2007), arXiv:hep-ph/0611147.
- [46] S. Roessner, C. Ratti, and W. Weise, Phys. Rev. **D 75**, 034007 (2007), arXiv:hep-ph/0609281.
- [47] E. Fraga and A. Mocsy, Braz. J. Phys. **37**, 281 (2007), arXiv:hep-ph/0701102.
- [48] B.-J. Schaefer, M. Wagner, and J. Wambach, Phys. Rev. **D 81**, 074013 (2010), arXiv:0910.5628 [hep-ph].
- [49] B. Schaefer and M. Wagner, Phys. Rev. **D 85**, 034027 (2012), arXiv:1111.6871 [hep-ph].
- [50] B. W. Mintz, R. Stiele, R. O. Ramos, and J. Schaffner-Bielich, Phys. Rev. **D 87**, 036004 (2013), arXiv:1212.1184 [hep-ph].
- [51] H. Gies and C. Wetterich, Phys. Rev. **D 69**, 025001 (2004), arXiv:hep-th/0209183.
- [52] J. M. Pawłowski, Annals Phys. **322**, 2831 (2007), arXiv:hep-th/0512261.
- [53] H. Gies, Lect. Notes Phys. **852**, 287 (2012), arXiv:hep-ph/0611146.
- [54] J. Braun, J. Phys. **G 39**, 033001 (2012), arXiv:1108.4449 [hep-ph].
- [55] L. M. Haas, J. Braun, and J. M. Pawłowski, AIP Conf. Proc. **1343**, 459 (2011), arXiv:1012.4735 [hep-ph].
- [56] K.-I. Kondo, Phys. Rev. **D 82**, 065024 (2010), arXiv:1005.0314 [hep-th].
- [57] T. K. Herbst, J. M. Pawłowski, and B.-J. Schaefer, Acta Phys. Polon. Suppl. **5**, 733 (2012), arXiv:1202.0758 [hep-ph].
- [58] H. Gies and C. Wetterich, Phys. Rev. **D 65**, 065001 (2002), arXiv:hep-th/0107221.
- [59] S. Floerchinger and C. Wetterich, Phys. Lett. **B 680**, 371 (2009), arXiv:0905.0915 [hep-th].
- [60] J. Greensite, Prog. Part. Nucl. Phys. **51**, 1 (2003), arXiv:hep-lat/0301023.
- [61] N. Weiss, Phys. Rev. **D 24**, 475 (1981).
- [62] D. J. Gross, R. D. Pisarski, and L. G. Yaffe, Rev. Mod. Phys. **53**, 43 (1981).
- [63] L. Fister and J. M. Pawłowski, (2011), arXiv:1112.5440 [hep-ph].
- [64] L. Fister and J. M. Pawłowski, (2011), arXiv:1112.5429 [hep-ph].
- [65] U. Ellwanger, M. Hirsch, and A. Weber, Z. Phys. **C 69**, 687 (1996), arXiv:hep-th/9506019.
- [66] B. Bergerhoff and C. Wetterich, Phys. Rev. **D 57**, 1591 (1998), arXiv:hep-ph/9708425.
- [67] J. M. Pawłowski, D. F. Litim, S. Nedelko, and L. von Smekal, Phys. Rev. Lett. **93**, 152002 (2004), arXiv:hep-th/0312324.
- [68] C. S. Fischer and H. Gies, JHEP **0410**, 048 (2004), arXiv:hep-ph/0408089.
- [69] C. S. Fischer, A. Maas, and J. M. Pawłowski, Annals Phys. **324**, 2408 (2009), arXiv:0810.1987 [hep-ph].
- [70] A. Dumitru, Y. Guo, Y. Hidaka, C. P. K. Altes, and R. D. Pisarski, Phys. Rev. **D 86**, 105017 (2012), arXiv:1205.0137 [hep-ph].
- [71] D. Diakonov, C. Gatttringer, and H.-P. Schadler, JHEP **1208**, 128 (2012), arXiv:1205.4768 [hep-lat].
- [72] C. Sasaki and K. Redlich, Phys. Rev. **D 86**, 014007 (2012), arXiv:1204.4330 [hep-ph].
- [73] M. Ruggieri, P. Alba, P. Castorina, S. Plumari, C. Ratti, *et al.*, Phys. Rev. **D 86**, 054007 (2012), arXiv:1204.5995 [hep-ph].
- [74] K. Fukushima and K. Kashiwa, (2012), arXiv:1206.0685 [hep-ph].
- [75] H. Reinhardt and J. Heffner, Phys. Lett. **B 718**, 672 (2012), arXiv:1210.1742 [hep-th].
- [76] K. Kashiwa and Y. Maezawa, (2012), arXiv:1212.2184 [hep-ph].
- [77] D. F. Litim and J. M. Pawłowski, , 168 (1998), arXiv:hep-th/9901063.
- [78] B.-J. Schaefer and J. Wambach, Phys. Part. Nucl. **39**, 1025 (2008), arXiv:hep-ph/0611191.
- [79] T. Hell, S. Roessner, M. Cristoforetti, and W. Weise, Phys. Rev. **D 79**, 014022 (2009), arXiv:0810.1099 [hep-ph].
- [80] K. Kashiwa, T. Hell, and W. Weise, Phys. Rev. **D 84**, 056010 (2011), arXiv:1106.5025 [hep-ph].
- [81] J. Beringer *et al.* (Particle Data Group), Phys. Rev. **D 86**, 010001 (2012).
- [82] J. Polonyi, Central Eur. J. Phys. **1**, 1 (2003), arXiv:hep-th/0110026.
- [83] B.-J. Schaefer, Phys. Atom. Nucl. **75**, 741 (2012), arXiv:1102.2772 [hep-ph].
- [84] L. von Smekal, Nucl. Phys. Proc. Suppl. **228**, 179 (2012), arXiv:1205.4205 [hep-ph].
- [85] V. Skokov, B. Friman, E. Nakano, K. Redlich, and B.-J. Schaefer, Phys. Rev. **D 82**, 034029 (2010), arXiv:1005.3166 [hep-ph].
- [86] G. Boyd, J. Engels, F. Karsch, E. Laermann, C. Legeland, *et al.*, Nucl. Phys. **B 469**, 419 (1996), arXiv:hep-lat/9602007.
- [87] O. Kaczmarek, F. Karsch, P. Petreczky, and F. Zantow, Phys. Lett. **B 543**, 41 (2002), arXiv:hep-lat/0207002.

- [88] S. Borsanyi, G. Endrodi, Z. Fodor, S. Katz, and K. Szabo, *JHEP* **1207**, 056 (2012), arXiv:1204.6184 [hep-lat].
- [89] B. W. Mintz, R. Stiele, R. O. Ramos, and J. Schaffner-Bielich, *AIP Conf. Proc.* **1520**, 370 (2013).
- [90] K. Fukushima and Y. Hidaka, *Phys. Rev. D* **75**, 036002 (2007), arXiv:hep-ph/0610323.
- [91] S. Borsanyi *et al.* (Wuppertal-Budapest Collaboration), *JHEP* **1009**, 073 (2010), arXiv:1005.3508 [hep-lat].
- [92] S. Borsanyi, G. Endrodi, Z. Fodor, A. Jakovac, S. D. Katz, *et al.*, *JHEP* **1011**, 077 (2010), arXiv:1007.2580 [hep-lat].
- [93] A. Bazavov, T. Bhattacharya, M. Cheng, C. DeTar, H. Ding, *et al.*, *Phys. Rev. D* **85**, 054503 (2012), arXiv:1111.1710 [hep-lat].
- [94] A. Bazavov (HotQCD Collaboration), *Nucl. Phys. A* (2012), arXiv:1210.6312 [hep-lat].
- [95] C. S. Fischer and J. Luecker, *Phys. Lett. B* **718**, 1036 (2013), arXiv:1206.5191 [hep-ph].
- [96] R. Stiele, L. M. Haas, J. Braun, J. M. Pawłowski, and J. Schaffner-Bielich, *PoS Confinement X*, 215 (2013), arXiv:1303.3742 [hep-ph].
- [97] D. Parganlija, P. Kovacs, G. Wolf, F. Giacosa, and D. H. Rischke, *Phys. Rev. D* **87**, 014011 (2013), arXiv:1208.0585 [hep-ph].